Structure-guided discovery of orexin receptor-binding PET ligands

Katharina Distler[1,2], Simone Maschauer[3], Eduard Neu[1,2], Harald Hübner[1,2], Jürgen Einsiedel[1,2], Olaf Prante[2,3], Peter Gmeiner[1,2*]

[1]Department of Chemistry and Pharmacy, Medicinal Chemistry, Friedrich-Alexander-Universität Erlangen-Nürnberg, Nikolaus-Fiebiger-Str. 10, 91058 Erlangen, Germany

[2]FAU NeW – Research Center New Bioactive Compounds, Friedrich-Alexander-Universität Erlangen-Nürnberg, Nikolaus-Fiebiger-Str. 10, 91058 Erlangen, Germany

[3]Department of Nuclear Medicine, Molecular Imaging and Radiochemistry, Friedrich-Alexander-Universität Erlangen-Nürnberg, Kussmaulallee 12, 91054 Erlangen, Germany

*Corresponding author: peter.gmeiner@fau.de

Keywords: G protein-coupled receptor, orexin receptor, ^{18}F-labeling, PET ligand

Abstract

Molecular imaging using positron emission tomography (PET) can serve as a promising tool for visualizing biological targets in the brain. Insights into the expression pattern and the *in vivo* imaging of the G protein-coupled orexin receptors OX1R and OX2R will further our understanding of the orexin system and its role in various physiological and pathophysiological processes. Guided by crystal structures of our lead compound **JH112** and the approved hypnotic drug suvorexant bound to OX1R and OX2R, respectively, we herein describe the design and synthesis of two novel radioligands, **[^{18}F]KD23** and **[^{18}F]KD10**. Key to the success of our structural modifications was a bioisosteric replacement of the triazole moiety with a fluorophenyl group. The ^{19}F-substituted analog **KD23** showed high affinity for the OX1R and selectivity over OX2R, while the high affinity ligand **KD10** displayed similar K_i values for both subtypes. Radiolabeling starting from the respective pinacol ester precursors resulted in excellent radiochemical yields of 93% and 88% for **[^{18}F]KD23** and **[^{18}F]KD10**, respectively, within 20 minutes. The new compounds will be useful in PET studies aimed at subtype-selective imaging of orexin receptors in brain tissue.

1. Introduction

Orexin receptors (OXR) belong to the class A of G protein-coupled receptors (GPCRs) and are categorized into two subtypes: orexin receptor type 1 (OX1R) and orexin receptor type 2 (OX2R). These receptors are activated by the neuropeptides orexin A (OXA) and orexin B (OXB).[1] While OXA exhibits similar binding affinities for both receptors, OXB has a preference for OX2R.[2] The human brain contains approximately 20,000-50,000 orexin-producing neurons originating in the lateral hypothalamus and extending into various brain areas.[1] Whereas the OX2R subtype plays a crucial role in modulating the sleep-wake rhythm and mutations in this receptor produce narcolepsy in animal models,[3-5] the OX1R subtype has a minor impact on sleep-wake regulation[2] and is primarily involved in modulating the reward system[6] and pain processing.[7, 8] To further examine the distinct role of OX1R, molecular imaging using positron emission tomography (PET) is a highly sensitive modality to study brain receptor densities *in vivo*.[9, 10] The development of a subtype selective OX1R radioligand for PET could facilitate the assessment of the regional OX1R expression in the central nervous system.[10, 11] Several OX2R-selective radioligands have been investigated[12-16]. However, these PET ligand candidates exhibited low brain uptake or high non-specific binding. Efforts to develop OX1R selective PET ligands (**Figure 1**) have faced equal challenges, such that [^{18}F]THIQ-1 and [^{18}F]THIQ-2[17] displayed low brain uptake, [^{18}F]PBC-1[18] exhibited unfavorable pharmacokinetic properties and [^{11}C]CW24[19] showed high non-specific binding in the brain.

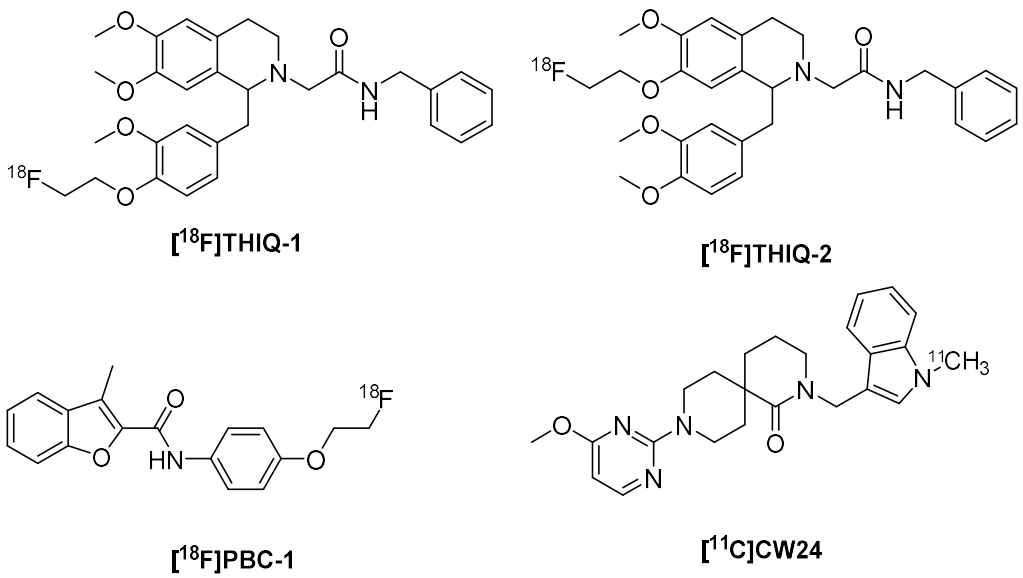

Figure 1. OX1R selective PET ligand candidates.

Herein, we describe the development of **[^{18}F]KD23**, a subtype-selective radioligand for OX1R, and its analog **[^{18}F]KD10** that specifically binds both subtypes, OX1R and OX2R. The structural design of **KD23** was based on our previously discovered OX1R-selective antagonist **JH112**,[20] a lead compound that is structurally related to the approved hypnotic drug suvorexant.[21] Both ligands adopt a horseshoe-like conformation within the binding pocket of OX1R, establishing particular interactions with the amino acids. The benzoxazole engages with residues C99$^{2.57}$, A102$^{2.60}$, S103$^{2.61}$, V106$^{2.64}$, W112$^{23.50}$, I122$^{3.28}$, P123$^{3.29}$, and Q126$^{3.32}$, while the homopiperazine interacts with A127$^{3.33}$, V130$^{3.36}$, Q179$^{4.60}$, M183$^{4.64}$, and F219$^{5.42}$. Additionally, the *meta*-toluamide forms interactions with S103$^{2.61}$, N318$^{6.55}$, H344$^{7.39}$, V347$^{7.42}$, and Y348$^{7.43}$, and the triazole interacts with Y311$^{6.48}$, I314$^{6.51}$, and S315$^{6.52}$. Subtype selectivity was designed guided by the crystal structures of OX1R (PDB: 4ZJ8)[22] and OX2R (PDB: 4S0V)[23] bound to suvorexant. There are only two sequence differences in the orthosteric binding sites within 4 Å of the ligand, conferring that the binding site of the OX2R subtype is ~30 Å^3 smaller than the binding site of OX1R.[20] The residue Ser103$^{2.61}$ of OX1R is exchanged for Thr111$^{2.61}$ in the OX2R. In addition, Ala127$^{3.33}$ of OX1R is replaced by the larger Thr135$^{3.33}$ for OX2R (numbers in superscript refer to the GPCRdb[24] (Ballesteros-Weinstein[25]) enumeration scheme). The binding pose revealed that the side chain in position 3.33 is located

in close proximity to the ethylene bridge of the central homopiperazine ring. Introduction of a *(S)*-*sec*-butyl substituent induced repulsive interactions with OX2R and thus subtype selectivity for OX1R (**Figure 2A**,**B**).[20] In contrast, the unsubstituted homopiperazine derivative (compound **17**[20]) can be harbored well by both receptor subtypes. Aiming to generate PET ligands, we carefully inspected the crystal structure of OX1R (PDB: 6V9S)[20] bound to **JH112** (**Figure 2B**). The size of the subpocket surrounding the five-membered triazole moiety of **JH112** indicated that the heteroarene may be replaced by a slightly larger fluorophenyl ring. Subsequent docking studies with the *meta*-fluorophenyl derivative, one of the possible regioisomers, suggested a stable binding pose, which was very similar to the binding pose of suvorexant and **JH112**. The fluorophenyl derivative **KD10** was designed as a ligand with high affinity for both OX1R and OX2R, whereas **KD23** demonstrated preferred binding to the OX1R. Hence, the ^{18}F-substituted analogs of the *meta*-fluorophenyl derivatives **KD10** and **KD23** appeared to be a promising approach toward potential PET ligands.

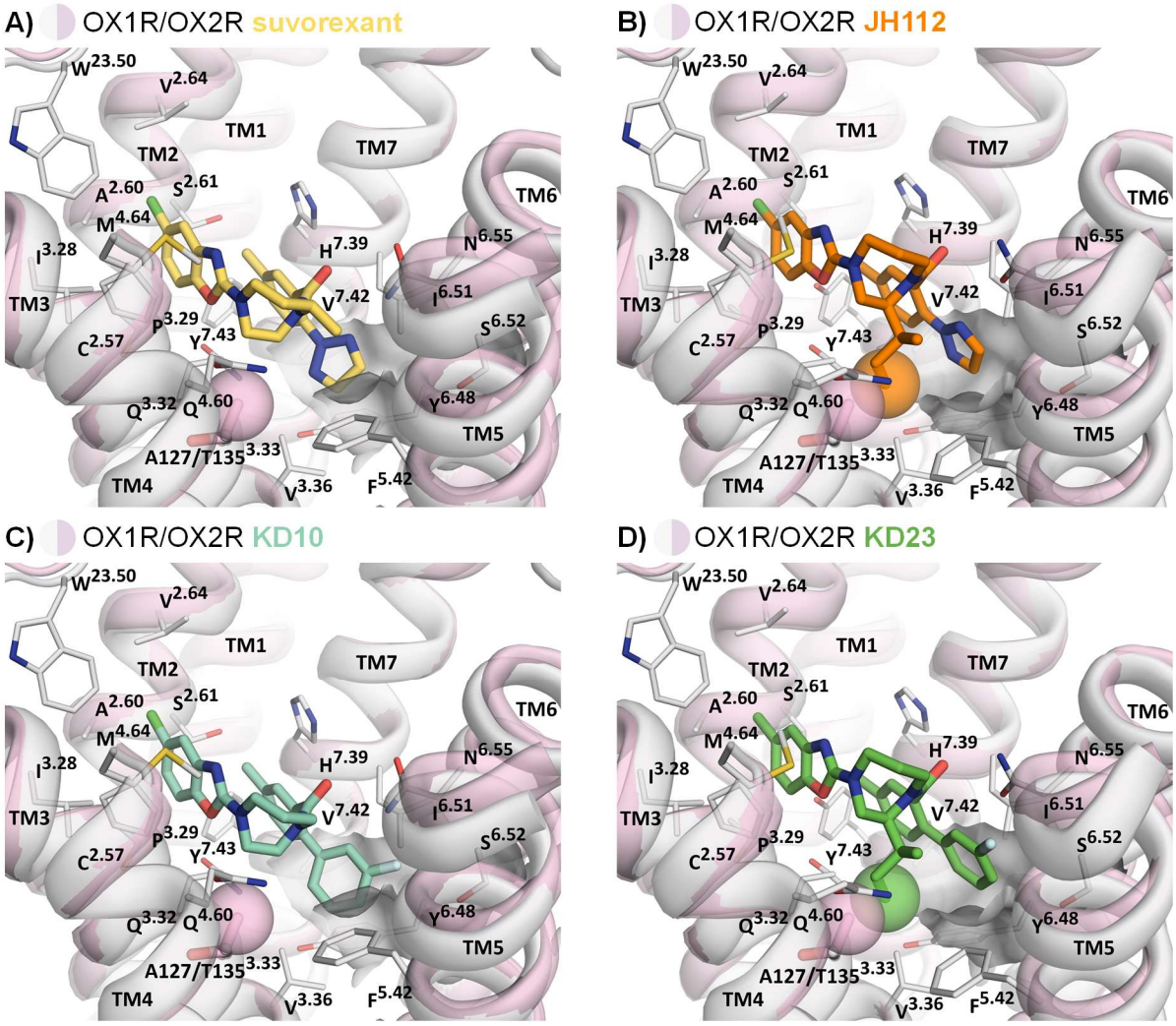

Figure 2. Structure-based design of selective and nonselective fluorine-substituted OXR ligands **KD23** and **KD10**, respectively. A, B) Suvorexant (yellow) and **JH112** (orange) are depicted within the binding pocket of OX1R (grey, PDB: 4ZJ8[22] for suvorexant, PDB: 6V9S[20] for **JH112**), with OX2R (pink, PDB: 4S0V[23]) superimposed for comparison. While suvorexant exhibits similar binding affinities for both subtypes OX1R and OX2R, the presence of the (*S*)-*sec*-butyl substituent in **JH112** induced repulsion with residue Thr135$^{3.33}$ in OX2R, resulting in distinct subtype selectivity for OX1R. C, D) Examination of the binding pocket's surface (grey) surrounding the triazole moiety revealed the potential for substitution with a slightly larger *meta*-fluorophenyl ring. The amino acids interacting with the ligands and forming the binding pocket of the OX1R are depicted as sticks. This substitution was implemented using the Builder Module of PyMOL[26] on the structures of suvorexant and **JH112**, resulting in the generation of **KD10** and **KD23**, respectively.

2. Results and discussion

2.1 Chemistry

To evaluate the receptor binding profiles of our new target compounds, we first performed the synthesis of the non-radioactive, ^{19}F-substituted compounds. Hence, we intended to synthesize the respective biphenylcarboxylic acids and subject those to an amide coupling with substituted or unsubstituted *N*-benzoxazolylhomopiperazines. Following an established protocol[27], we prepared the different regioisomers of the fluorobiphenylcarboxylic acids using a two-step procedure. First, the carbon-carbon bond of the biaryl system was formed by a Suzuki cross-coupling reaction of 2-iodo-5-methyl benzoate (**1**) with *ortho*- and *meta*-fluorophenylboronic acid or its *para*-pinacol ester derivative. Subsequent saponification under basic conditions yielded the regioisomers **2.1**, **3.1**, and **4.1** (88-94% yield) (**Scheme 1**).

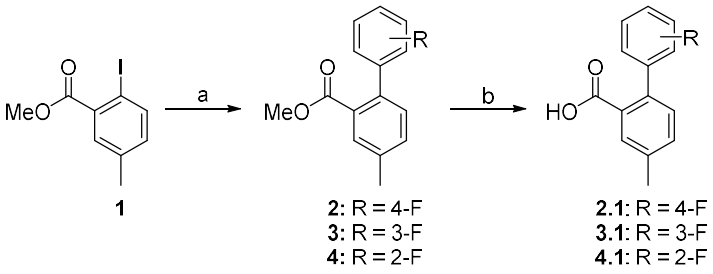

Scheme 1. Synthesis of fluoro-substituted biphenylcarboxylic acids: a) boronic acid derivative (**2**: 4-F-Ph-$BO_2C_6H_{12}$, **3**: 3-F-Ph-$B(OH)_2$, **4**: 2-F-Ph-$B(OH)_2$), $PdCl_2(PPh_3)_2$, Na_2CO_3, THF, 80 °C, 12 h; b) 1 M NaOH, MeOH, 50 °C, 12 h, **2.1**: 94%, **3.1**: 91%, **4.1**: 88%.

We prepared the homopiperazine building blocks **5**[20] and **13**[20] by a Cu(II)-catalyzed CH-amination of 5-chlorobenzo[*d*]oxazole with *N*-Boc protected homopiperazine, followed by the cleavage of the Boc protection group under acidic conditions.[20] The chiral *sec*-butyl substituted homopiperazine precursor was prepared starting from (*S*)-isoleucine following our recently described protocol.[20] Previous structure-activity relationship (SAR) studies indicated the importance of the methyl group attached to the triazolylbenzamide moiety for orexin receptor binding affinity.[22] To elucidate the relevance of this methyl group as a part of the biphenyl

system, the non-fluorinated congeners **8** and **9** were synthesized by a HATU-promoted acylation of the homopiperazine derivative **5** with the biphenylcarboxylic acids **6** and **7**. Analogously, the fluoro-substituted biphenyl derivatives **10**, **11 (KD10)**, and **12** were prepared starting from the carboxylic acid derivatives **2.1**, **3.1**, and **4.1**. Employing the chiral homopiperazine derivative **13**, HATU-mediated coupling of **3.1** and **4.1** required elevated temperature, due to the bulky *sec*-butyl substituent. Nevertheless, the amide derivatives **14 (KD23)** and **15** were formed in 60% and 65% yield, respectively (**Scheme 2**). Noteworthy, the bulky substituent was responsible for the formation of rather stable rotamers of both **KD23** and **15**, which resulted in a peak splitting in the HPLC-chromatograms, apparently caused by an exceptionally high rotation barrier of the amide bond. This phenomenon was not observed for the *C*-unsubstituted homopiperazine derivatives **8-12**.

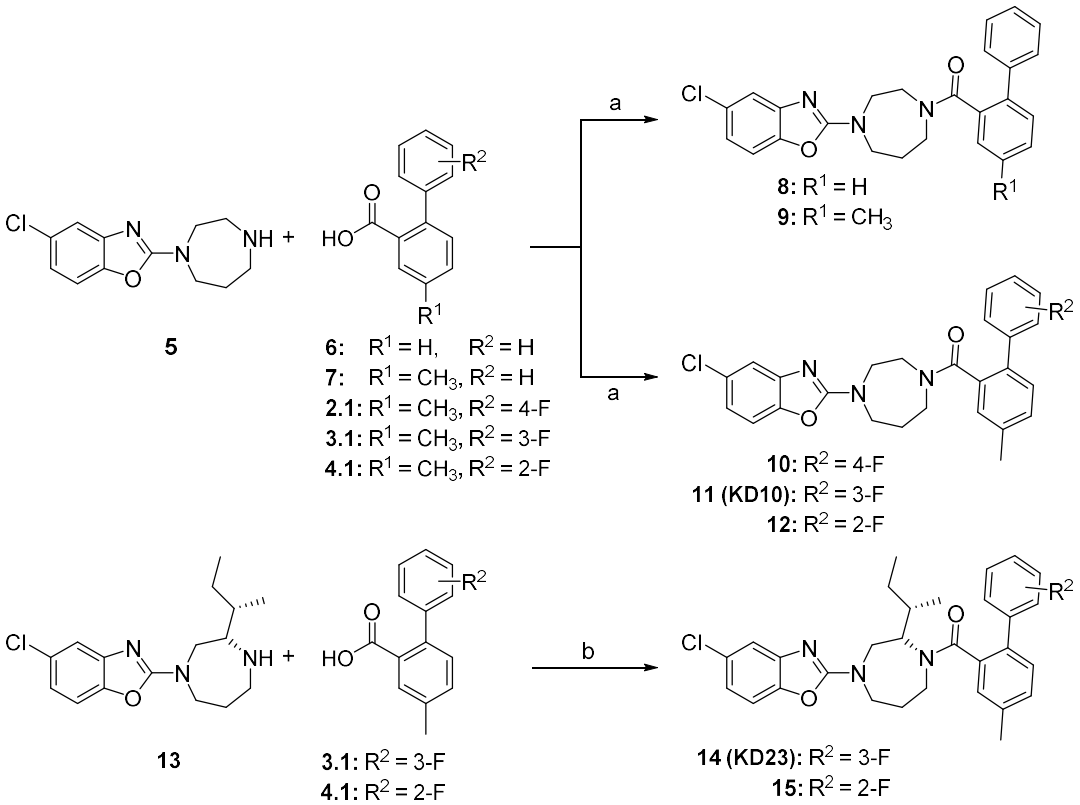

Scheme 2. Synthesis route for the unselective and OX1R-selective antagonists: a) 1) **6**, **7**, **2.1**, **3.1**, or **4.1**, HATU, DIPEA, DMF, rt, 10 min, 2) **5**, rt, 2 h, **8**: 85%, **9**: 91%, **10**: 89%, **11 (KD10)**: 93%, **12**: 90%; b) 1) **3.1**, or **4.1**, HATU, DIPEA, DMF, rt, 20 min, 2) **13**, 50 °C, 12 h, **14 (KD23)**: 60%, **15**: 65%.

We envisioned the ^{18}F-labeled target compounds **[^{18}F]KD10** and **[^{18}F]KD23** by radiofluorination of suitable boronic acid pinacol esters. Thus, we conducted a Suzuki cross-coupling reaction of the building block **1** with 3-bromophenylboronic acid pinacol ester (**Scheme 3**). The biphenyl derivative **16** was saponified under basic conditions to obtain the carboxylic acid **17**. HATU-promoted coupling reactions with the homopiperazines **5** and **13** were done at elevated temperature to furnish the 3'-bromobiphenyl carboxamide derivatives **18** and **19**, respectively. Subjection to bis(pinacolato)diboron in the presence of the palladium catalyst $PdCl_2(dppf)\times CH_2Cl_2$ allowed the conversion of the intermediates **18** and **19** to give the arylboronic acid ester derivatives **20** and **21**, respectively. To take advantage of the promising OXR binding properties of **KD10** and **KD23** (**Table 2**), and to demonstrate the accessibility of the ^{18}F-substituted analogs **[^{18}F]KD10** and **[^{18}F]KD23** as potential PET ligands, initial ^{18}F-labeling experiments on an analytical scale were performed starting from the boronic acid pinacol (BPin) esters **20** and **21**. Applying the well-established alcohol-enhanced copper-mediated radiofluorination method[9], both BPin precursors, **20** and **21**, were reacted with [^{18}F]fluoride in the presence of copper(II) triflate in DMA/*n*-butanol at 110 °C. The reaction conditions have been optimized for the reaction volume to allow radiolabeling in high radiochemical yield (RCY) with only 7.1 µmol of the respective BPin precursor, carefully considering a BPin precursor-to-$[Cu(OTf)_2py_4]$ ratio of 1:1[28] (**Scheme 3**).

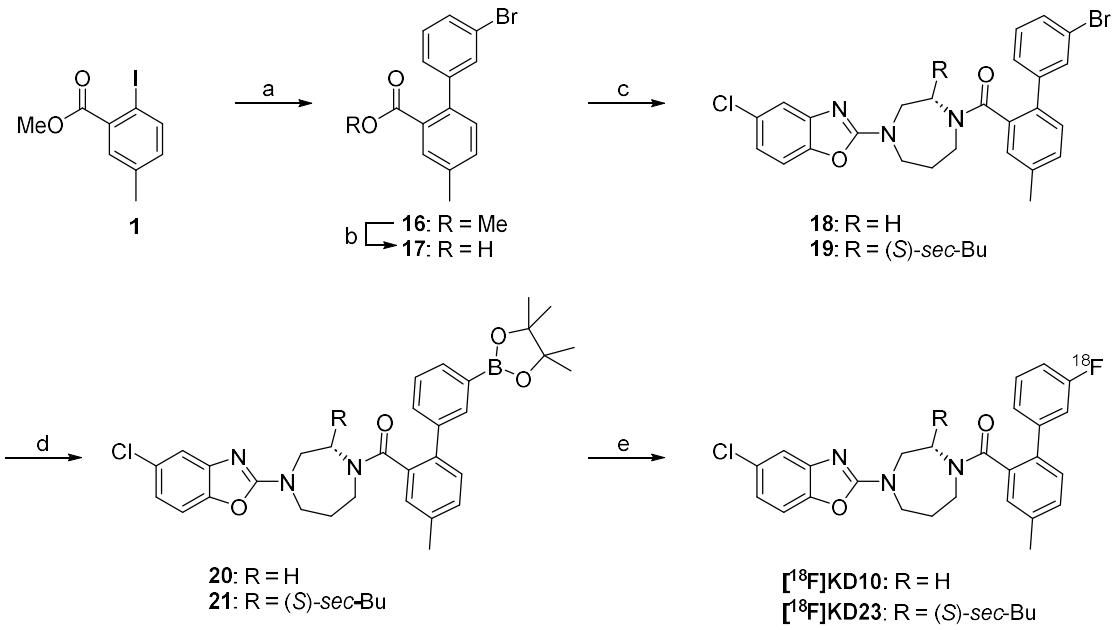

Scheme 3. Synthesis route for radioligands **[^{18}F]KD10** and **[^{18}F]KD23**: a) 3-Br-Ph-$BO_2C_6H_{12}$, Na_2CO_3, THF, 80 °C, 2 h, **16**: 69%; b) 2 M NaOH, MeOH, dioxane, 60 °C, 12 h, **17**: 95%; c) 1) **17**, HATU, DIPEA, DMF, rt, 20 min, 2) for **18**: **5**, for **19**: **13**, 50 °C, 12 h, **18**: 86%, **19**: 65%; d) bis(pinacolato)diboron, $PdCl_2$(dppf)×CH_2Cl_2, KOAc, dioxane, 80 °C, **20**: 69% **21**: 63%; e) tetraethylammonium [^{18}F]fluoride, tetrakis(pyridine)copper(II) triflate, DMA/*n*-butanol (2:1, v/v), 20 min, 110 °C.

The time dependence of the ^{18}F-fluorination showed the typical course of a Cu-mediated ^{18}F-substitution, reaching the maximum RCY for **[^{18}F]KD10** and **[^{18}F]KD23** of 88% and 93%, after 20 min (**Table 1**). Interestingly, earlier investigations on benzoxazole-5-BPin ester precursors showed that the copper-mediated ^{18}F-substitution gave a limited RCY of only 20-30%.[28] Our approach of introducing ^{18}F with a fluorophenyl substituent, replacing the triazole ring in the lead compounds **JH112** and its *C*-nonsubstituted analog, turned out to be highly promising, as the ^{18}F-labeling provided **[^{18}F]KD23** and **[^{18}F]KD10** with high RCYs. Future work will be directed to an upscaling of the radiosynthesis, enabling the evaluation of **[^{18}F]KD23** and **[^{18}F]KD10** as potential PET ligands to study OX1R and OX2R expression in further *in vitro* and *in vivo* experiments.

Table 1. Time dependency of the radiochemical yields for the copper-mediated ^{18}F-fluorination of **20** and **21**, respectively, to afford **[^{18}F]KD10** and **[^{18}F]KD23** (reaction conditions: see **Scheme 3**).

t (min)	RCY (%)	
	[^{18}F]KD10	**[^{18}F]KD23**
2	20	22
5	62	53
10	82	85
20	88	93

2.2 Radioligand binding experiments

Receptor binding affinities of the test compounds have been determined in a radioligand displacement assay.[20, 29] Membranes of HEK 293T cells transiently expressing the human OX1R or OX2R were used for dose-response experiments to determine K_i values for the ligands in comparison to the reference agent **JH112** (**Table 2**). Apart from compound **8**, all biphenyl derivatives showed one-digit nanomolar affinities for OX1R (from 1.3 nM for **12** to 6.4 nM for **10**), confirming that the substitution of the triazole with a fluorophenyl ring is well tolerated by OX1R. K_i values of the non-fluorinated compounds with and without the methyl group (**9**: 1.8 nM, and **8**: 21 nM) emphasize the importance of the methyl group attached to the carboxylic acid moiety for OX1R binding affinity. Maintaining the methyl substituent and introducing a fluoro substituent in *ortho*-, *meta*-, and *para*-position (**12**: 1.3 nM, **KD10**: 2.3 nM, and **10**: 6.4 nM) did not affect binding affinity, but indicated a preference for the *ortho*- and *meta*-position. Since these compounds lack the *sec*-butyl substituent in position 2 of the homopiperazine, they revealed high affinity for both subtypes. In contrast, the *sec*-butyl substituted *ortho*- and *meta*-analogs **15** and **KD23** showed a 25- and 32-fold selectivity for OX1R over OX2R with K_i values of 3.4 nM and 2.8 nM respectively. Therefore, **KD10** and **KD23** proved to be promising candidates for ^{18}F-labeling. Remarkably, the bromo analog of **KD23**, compound **19**, which was synthesized as an intermediate for ^{18}F-labeling of **21**, showed

a 100-fold selectivity for OX1R over OX2R with K_i values of 3.4 nM (OX1R) and 340 nM (OX2R).

To investigate if the newly developed ligands are agonists or antagonists, we performed an IP accumulation assay reflecting OX1R-mediated $G\alpha_q$-protein signaling[20] for the three representative ligands **KD10**, **KD23** and **19**. In fact, the test compounds did not activate OX1R but completely inhibited the effect of 30 nM orexin A with inhibition constants of 68 nM for **KD23** and 160 nM for **KD10** and **19** (**SI**, **Table S1**, **Figure S1**). As **JH112** revealed an IC_{50} = 17 nM these data are in good agreement with the binding affinities (**Table 2**). Hence, the test compounds clearly behaved as OX1R antagonists.

Table 2: Receptor binding affinities of the orexin receptor ligands **8**-**10, 12**, **15**, **18**, **19**, **KD10** and **KD23** in comparison to the lead compound **JH112** to the human receptor subtypes OX1R and OX2R.

compd.	K_i values [nM ± S.E.M.][a]				selectivity for OX1R over OX2R[e]
	OX1R[b]	n[c]	OX2R[d]	n[c]	
8	21 ± 2.7	3	5.3 ± 1.3	4	0.25
9	1.8 ± 0.18	3	2.5 ± 0.23	3	1.4
10	6.4 ± 0.18	3	7.4 ± 1.6	3	1.2
KD10	2.3 ± 0.55	4	1.6 ± 0.21	5	0.70
12	1.3 ± 0.17	3	1.6 ± 0.16	4	1.2
KD23	2.8 ± 0.32	9	90 ± 8.1	10	32
15	3.4 ± 0.63	5	86 ± 12	4	25
18	3.2 ± 0.87	6	15 ± 3.3	5	4.7
19	3.4 ± 0.63	8	340 ± 60	8	100
JH112[20]	0.72 ± 0.08	6	54 ± 7.0	6	75

[a] K_i values in nM ± S.E.M. are means of single experiments each done in triplicate. [b] Membranes from HEK293T cells transiently expressing the human OX1R were incubated with the radioligand [^{3}H]SB974042. [c] Number of individual experiments. [d] Homogenates from HEK293T cells which transiently express the human OX2R were incubated with the radioligand [^{3}H]EMPA. [e] Ratio of subtype selectivity calculated by dividing K_i for OX2R by the K_i for OX1R.

2.3 Computational analysis

Previous drug discovery studies demonstrated that small modifications of a lead compound could result in a substantial change of the binding mode.[30-32] In the GPCR field, the serotonin receptor subtypes 5-HT_{1A}R and 5-HT_{2A}R displayed the complexity of different ligand binding modes when an identical drug proved two clearly different binding modes.[33, 34] To investigate the binding mode of **KD23** and its interactions with the OX1R, we conducted docking experiments utilizing the previously reported **JH112**-bound OX1R crystal structure as a template.[20] Core-constrained docking with **JH112** as a reference, employing a tolerance of 2 Å, was performed to maintain the horseshoe-like conformation and allow ample exploration of the binding site. Remarkably, docking yielded two predominant binding modes for **KD23** (**Figure 3**). The first, which we term the canonical binding mode (**Figure 3A**), shows **KD23** adopting a conformation reminiscent of **JH112** showing interactions analogously to **JH112** as described above. In the second noncanonical binding mode (**Figure 3B**), the benzoxazole and homopiperazine moieties adopt a conformation similar to that observed in the **JH112**-bound structure. The main difference is the torsion of the biphenyl moiety by approximately 180 ° causing alternative interactions of the *meta*-toluamide with $Y311^{6.48}$, $I314^{6.51}$ and $N318^{6.55}$, while the 3-fluorophenyl interacts with $S103^{2.61}$, $H344^{7.39}$, $V347^{7.42}$, and $Y348^{7.43}$. Particularly intriguing are the π-stacking interactions observed. In the canonical conformation, the 3-fluorophenyl engages in an edge-to-face interaction with $F219^{5.42}$ and parallel staggered π-stacking with $Y311^{6.48}$, while in the noncanonical conformation, a robust face-to-face π-stacking interaction between the benzoxazole, the fluorophenyl, and $H344^{7.39}$ is established. Interestingly, such a face-to-face π-stacking has also been observed in the structures of lemborexant and the urea derivatives SB-334867 and SB-408124.[35]

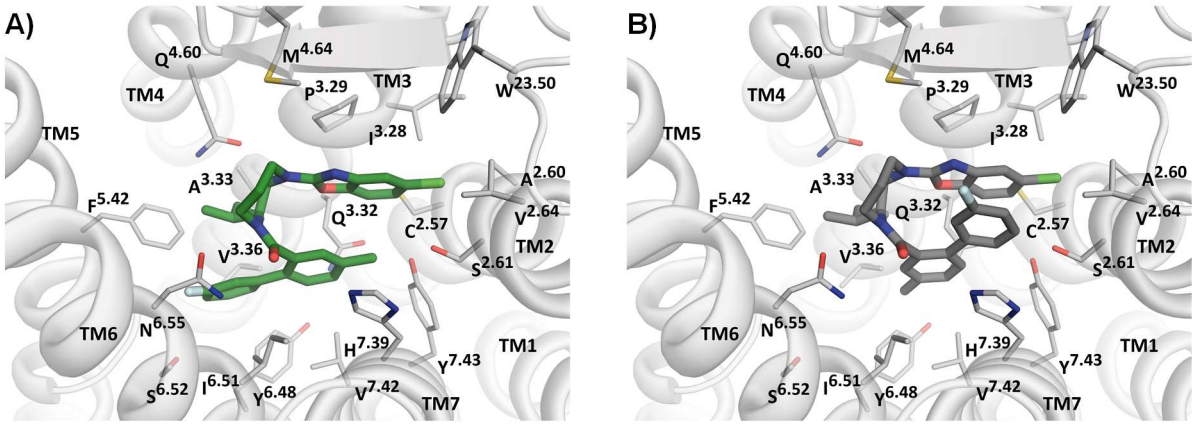

Figure 3. Comparison of different **KD23** binding modes at the OX1R. Docking of **KD23** into the **JH112**-bound OX1R structure (PDB: 6V9S)[20] generated two distinctively different binding modes. A) In the canonical binding mode (green) the binding of **KD23** resembles **JH112**. B) In the noncanonical binding mode (grey), the biphenyl moiety is flipped by almost 180°.

Based on the ambiguity of the different conformations and to learn more about the preferred position of the fluoro substituent, molecular dynamics (MD) simulations were applied to investigate the relevance of this observation in more detail and determine the most stable binding mode. Due to the restricted rotation of the biphenyl moiety for both binding modes, simulations were started in which the fluoro substituent is either pointing towards the extracellular side, or towards the intracellular side. Interestingly, the MD simulations demonstrated a lower root-mean-square fluctuation (RMSF) for the heavy atoms of **KD23** in the canonical binding conformation with the fluoro substituent directed towards the extracellular site (**SI, Figure S4**) confirming the canonical binding mode of the docking studies. Furthermore, MD simulations to investigate the subtype selectivity of compound **19** revealed that the steric demand of the bromo substituent leads to a shift of the molecule towards TM2 likely causing repulsive interactions with T111$^{2.61}$ of OX2R, thereby contributing to the generation of subtype selectivity for OX1R **(SI, Figure S4, S5, S6)**.

3. Conclusion

In this study, we report on a structure-guided development of the radioligands **[^{18}F]KD23** and **[^{18}F]KD10**. Whereas the ^{19}F-substituted analog **KD23** showed nanomolar binding affinity and 30-fold selectivity for the orexin receptor type 1 (OX1R), the K_i values of its analog **KD10** reflect high affinity for both subtypes OX1R and OX2R. Starting from the pinacol esters **21** and **20** as precursors, ^{18}F-radiolabeling was associated with excellent radiochemical yields of 93% and 88%, respectively, within 20 minutes. These promising results provide a solid basis for further *in vitro* and *in vivo* experiments with this potential PET ligand pair to study their pharmacokinetics and imaging properties. A direct comparison of the OX1R-selective ligand **[^{18}F]KD23** with the nonselective ligand **[^{18}F]KD10** may provide valuable information on the role of both OXR subtypes in future *in vivo* studies with the perspective of advancing our understanding of the orexin system and its role in various physiological and pathophysiological processes.

4. Experimental section

4.1 Chemistry

Reagents and solvents were purchased in their purest grade from abcr, Acros, Alfa Aesar, Sigma Aldrich, Apollo Scientific, Fisher Scientific, and BLD Pharm and were used without further purification. Unless otherwise noted, reactions were performed using dry solvents under a nitrogen or argon atmosphere. Thin-layer chromatography (TLC) was performed using aluminium sheets coated with Merck 60 F_{254}, or Merck 60 RP-18 F_{254} silica gel, and the spots were visualized under UV light (254 nm). Purification by flash chromatography was performed using silica gel 60 (40-63 µm mesh), from Merck, or RP-18 silica gel (50 µm mesh) from YMC as a stationary phase on a Biotage Selekt automated flash purification system with a UV-Vis detector. Purification by preparative HPLC was performed on an Agilent 1260 infinity system

using an Agilent Zorbax XDB-C8 column (21.2 mm × 150 mm, 5 µm) (column 1) or an Agilent Eclipse XDB-C8 column (30 mm × 150 mm, 5 µm) (column 2). Compounds were characterized by NMR spectroscopy and high-resolution mass spectrometry (HRMS) for chiral by optical rotation. NMR spectra were obtained on a Bruker Avance 400 (400 MHz for ^{1}H and 101 MHz for ^{13}C) or a Bruker Avance 600 (600 MHz for ^{1}H and 151 MHz for ^{13}C) spectrometer at 298 K using the solvents indicated. Chemical shifts are reported relative to TMS, or to the residual solvent peak, for DEPTQ spectra relative to the corresponding solvent peaks, 77.16 ppm for $CDCl_3$ and 39.52 ppm for DMSO-d_6. ESI-mass spectra were recorded using LC-MS: Thermo Scientific Dionex Ultimate 3000 UHPLC quarternary pump, autosampler and RS-diode array detector, column: Zorbax-Eclipse XDB-C8 analytical column (3.0 mm × 100 mm, 3.5 µm), flow rate 0.4 mL/min using DAD detection (230 nm; 254 nm), coupled to a Bruker Daltonics Amazon mass spectrometer. High mass accuracy and resolution experiments were performed on a Bruker Daltonics timsTOF Pro spectrometer using electrospray ionization (ESI) as an ionization source. The purity of all test compounds and key intermediates was determined by reverse phase HPLC. HPLC analysis was performed on analytical systems (Agilent 1100 analytical series, VWD detector), Zorbax Eclipse XDB-C8 analytical column (4.6 mm × 150 mm, 5 µm), flow rate: 0.5 mL/min; system 1: CH_3CN/0.1% aq. TFA, gradient: 3% to 85% CH_3CN in 26 min, 85% to 95% CH_3CN in 2 min, 95% CH_3CN for 2 min; system 2: CH_3CN/0.1% aq. TFA, gradient: 3% to 95% CH_3CN in 28 min, 95% CH_3CN for 2 min; system 3: CH_3CN/0.1% aq. TFA, gradient: 20% to 95% CH_3CN in 15 min, 95% CH_3CN for 2 min. Optical rotation measurements were performed, using a JASCO P-2000 polarimeter with a class cuvette (path length: 100 mm, volume: 1.2 mL) A filtered sodium lamp (589 nm) generated linearly polarized light and the obtained data was analyzed using the *Jasco Spectra Manage*r software. Radio-HPLC was performed on an Agilent 1100 system (Agilent Technologies) with a quaternary pump and variable wavelength detector and a radio-HPLC detector (HERM LB 500, Berthold Technologies, Germany) on a Chromolith RP-18e column (RP, 100 × 4.6 mm, 5 µm particle size, flow rate: 4 mL/min) using a linear gradient from 10–100% acetonitrile (0.1% TFA) in water (0.1% TFA) over 5 min. All ^{18}F-labeled

compounds were identified via the retention time (t_R) of their non-radioactive reference compounds (**SI, Figure S2 and S3**). No-carrier-added (n.c.a.) [^{18}F]fluoride was produced through the ^{18}O(p,n)^{18}F reaction on a PETtrace 800 cyclotron (General Electric, Uppsala, Sweden) using H_2[^{18}O]O as the target and purchased from Universitätsklinikum Würzburg, Klinik und Poliklinik für Nuklearmedizin, Germany.

4.2 Synthesis

[^{18}F]KD10 and **[^{18}F]KD23**: Copper-mediated ^{18}F-fluorination

The ^{18}F-labeling of BPin ester precursors **20** and **21** was performed following the procedure described by Shinde et al.[28]. The [^{18}F]fluoride in aqueous solution was passed through a Sep-Pak® Light (46 mg) Accel™ Plus QMA carbonate cartridge from the male side. The cartridge was washed with acetone (dry, 2 mL) from the male side, and air (10 mL) was passed over the cartridge from the female side to remove residual water. [^{18}F]Fluoride was eluted into a preheated (85 °C) reaction vial applying a solution of tetraethylammonium bicarbonate (TEAB) in dry methanol (6.2 mM, 500 µL). A stream of helium was used to remove the solvent, the reaction vial was heated to 110 °C and a solution of the respective BPin ester (7.1 µmol, **20** or **21**) and tetrakis(pyridine)copper(II) triflate ([Cu(OTf)$_2$py$_4$], 6.4 µmol)) in dimethylacetamide (DMA) and *n*-butanol (2:1, 200 µL) was added. The reaction mixture was stirred for 20 min under air and samples were drawn for radio-HPLC analysis (see 4.1 and Supplementary data), to monitor the formation of ^{18}F-labeled **[^{18}F]KD10** and **[^{18}F]KD23**, respectively.

4'-Fluoro-4-methyl-[1,1'-biphenyl]-2-carboxylic acid (**2.1**)[36]

To a solution of 4-fluorophenylboronic acid pinacol ester (84 µL, 0.398 mmol) in THF (1 mL) was added $PdCl_2(PPh_3)_2$ (7.63 mg, 0.011 mmol) and then an aqueous solution of Na_2CO_3 (1 mL, 0.8 M). After stirring for 2 min at rt, methyl 2-iodo-5-methylbenzoate (**1**, 60 µL,

0.362 mmol) was added. After stirring at 80 °C for 12 h, extraction was done with ethyl acetate, the organic layer was washed with brine, dried over anhydrous Na_2SO_4, and concentrated under reduced pressure. Purification was done by automated flash chromatography (ethyl acetate/isohexane: gradient 6-15% ethyl acetate) to obtain methyl 4'-fluoro-4-methyl-[1,1'-biphenyl]-2-carboxylate (**2**) as a transparent oil. The crude compound was dissolved in methanol (3 mL) and an aqueous solution of NaOH (3 mL, 1 M) was added. After heating the reaction mixture at 50 °C for 12 h, the methanol fraction was removed under reduced pressure and pH 3 was adjusted with 6 M HCl. Extraction with ethyl acetate was performed and the organic layer was washed with brine, dried over Na_2SO_4, and the solvent was removed under reduced pressure to yield compound **2.1** as a white solid (78.5 mg, 94%), which was used without further purification. ^{1}H-NMR (400 MHz, $CDCl_3$): δ (ppm) 7.79-7.76 (m, 1H), 7.37 (ddq, J = 7.8, 1.9, 0.6 Hz, 1H), 7.29-7.23 (m, 2H), 7.23-7.20 (m, 1H), 7.09-7.02 (m, 2H), 2.42 (bs, 3H); ^{13}C-NMR (DEPTQ, 101 MHz, $CDCl_3$): δ (ppm) 173.3, 162.4 (d, J = 246 Hz), 139.8, 137.5, 137.1 (d, J = 3 Hz),133.1, 131.4, 131.3, 130.2 (d, J = 8 Hz), 129.0, 115.1 (d, J = 21 Hz), 21.0; ESI-MS: *m/z* 231.0 $[M+H]^+$. Analytical data were in accordance with those reported in the literature [36].

3'-Fluoro-4-methyl-[1,1'-biphenyl]-2-carboxylic acid (**3.1**)[36]

The synthesis, workup and purification of compound **3.1** was performed as described for **2.1**, employing 3-fluorophenylboronic acid (121.6 mg, 0.869 mmol) in THF (1 mL), $PdCl_2(PPh_3)_2$ (15.3 mg, 0.022 mmol), an aqueous solution of Na_2CO_3 (2 mL, 0.8 M) and methyl 2-iodo-5-methylbenzoate (**1**, 120 µL, 0.724 mmol) and, finally, methanol (3 mL) and an aqueous solution of NaOH (3 mL, 1 M) for saponification of **3** to yield compound **3.1** as a white solid (152.4 mg, 91%), which was used without further purification. ^{1}H-NMR (400 MHz, $CDCl_3$): δ (ppm) 7.78-7.75 (m, 1H), 7.38 (ddq, J = 7.8, 1.9, 0.6 Hz, 1H), 7.36-7.28 (m, 1H), 7.23 (d, J =

7.7 Hz, 1H), 7.08 (ddd, *J* = 7.6, 1.4, 1.2 Hz, 1H), 7.06-7.00 (m, 2H), 2.43 (brs, 3H); ^{13}C-NMR (DEPTQ, 101 MHz, $CDCl_3$): *δ* (ppm) 172.8, 162.5 (d, *J* = 245 Hz), 143.4 (d, *J* = 8 Hz), 139.5 (d, *J* = 2 Hz), 137.8, 133.1, 131.5, 131.1, 129.6 (d, *J* = 8 Hz), 128.9, 124.5 (d, *J* = 3 Hz), 115.7 (d, *J* = 22 Hz), 114.2 (d, *J* = 21 Hz), 21.0; ESI-MS: *m/z* 231.0 $[M+H]^+$. Analytical data were in accordance with those reported in the literature [36].

2'-Fluoro-4-methyl-[1,1'-biphenyl]-2-carboxylic acid (**4.1**)

The synthesis, workup and purification of compound **4.1** was performed as described for **2.1**, employing 2-fluorophenylboronic acid (60.8 mg, 0.435 mmol) in THF (1 mL), $PdCl_2(PPh_3)_2$ (7.6 mg, 0.011 mmol), an aqueous solution of Na_2CO_3 (1 mL, 0.8 M) and methyl 2-iodo-5-methylbenzoate (**1**, 60 µL, 0.362 mmol) and, finally, methanol (3 mL) and an aqueous solution of NaOH (3 mL, 1 M) for saponification of **4** to yield compound **4.1** as a white solid (73.6 mg, 88%), which was used without further purification. Analytical HPLC (220 nm): system 1, purity: >99% (t_R: 19.9 min); ^{1}H-NMR (400 MHz, $CDCl_3$): *δ* (ppm) 7.87 (dq, *J* = 2.2, 0.6 Hz, 1H), 7.42 (ddq, *J* = 7.8, 2.2, 0.7 Hz), 7.32 (dddd, *J* = 8.2, 7.3, 5.2, 1.9 Hz, 1H), 7.28 (dddd, *J* = 7.6, 7.6, 1.9, 0.3 Hz, 1H), 7.24 (dq, *J* = 7.8, 0.3 Hz, 1H), 7.18 (ddd, *J* = 7.6, 7.3, 1.2 Hz, 1H), 7.06 (dddd, *J* = 10.1, 8.2, 1.2, 0.3 Hz, 1H), 2.44 (ddd, *J* = 0.7, 0.6, 0.3 Hz); ^{13}C-NMR (DEPTQ, 151 MHz, $CDCl_3$): *δ* (ppm) 172.3, 159.7 (d, *J* = 246 Hz), 138.1, 134.3, 133.5, 131.8, 131.5, 130.5 (d, *J* = 4 Hz), 129.4, 129.3 (d, *J* = 8 Hz), 129.0 (d, *J* = 16 Hz) 124.1 (d, *J* = 4 Hz), 115.2 (d, *J* = 22 Hz), 21.1; ESI-MS: *m/z* 231.0 $[M+H]^+$; HR-ESI-TOF-MS $[M+H]^+$ calcd. for $C_{14}H_{12}FO_2$: 231.0816, found: 231.0816.

[1,1'-Biphenyl]-2-yl(4-(5-chlorobenzo[*d*]oxazol-2-yl)-1,4-diazepan-1-yl)methanone (**8**)

To a solution of [1,1'-biphenyl]-2-carboxylic acid (**6**, 51.4 mg, 0.259 mmol) and HATU (156.7 mg, 0.412 mmol) in DMF (3 mL) was added DIPEA (170 µL, 0.983 mmol). After stirring

for 10 min at rt, 5-chloro-2-(1,4-diazepan-1-yl)benzo[*d*]oxazole (**5**, 50.9 mg, 0.202 mmol) in DMF (1 mL) was added and the solution was reacted for 2 h at rt. Upon dilution with ethyl acetate and washing with saturated aqueous sodium bicarbonate solution and brine, the organic layer was dried over Na_2SO_4, filtered and the solvent was removed under reduced pressure. Purification was done by preparative HPLC using CH_3CN/0.1% aq. TFA, a gradient of 3-85% CH_3CN in 26 min (column 1, t_R = 21.8 min, λ = 220 nm) at a flow rate of 12 mL/min to obtain compound **8** as a white solid (74.3 mg, 85%). Analytical HPLC (220 nm): system 1, purity: >99% (t_R: 23.1 min); ^{1}H-NMR (400 MHz, $CDCl_3$, several rotamers were observed): *δ* (ppm) 7.53-7.46 (m, 3H), 7.46-7.38 (m, 2H), 7.38-7.29 (m, 3H), 7.24-7.13 (m, 2H), 7.11 (d, *J* = 8.5 Hz, 0.5H), 7.05 (dd, *J* = 8.4, 2.1 Hz, 0.5H), 7.01 (dd, *J* = 8.5, 2.1 Hz, 0.5H), 6.95-6.88 (m, 0.5H), 4.42-4.12 (m, 0.5H), 3.86-3.76 (m, 1H), 3.74-3.65 (m, 1H), 3.65-3.56 (m, 1H), 3.55-3.48 (m, 1H), 3.47-3.38 (m, 1H), 3.33-3.24 (m, 1H), 3.08-2.97 (m, 1H), 2.89-2.78 (m, 0.5H), 2.23-2.03 (m, 0.5H), 1.92-1.76 (m, 0.5H), 1.62-1.47 (m, 0.5H), 1.21-1.05 (m, 0.5H); ^{13}C-NMR (DEPTQ, 151 MHz, $CDCl_3$, several rotamers were observed): *δ* (ppm) 171.70, 171.67, 162.0, 161.9, 147.1, 146.9, 143.3, 142.7, 139.9, 139.6, 138.3, 135.2, 130.1, 130.0, 129.80, 129.77, 129.7, 129.1, 129.0, 128.7, 128.5, 128.1, 128.0, 127.9, 127.8, 127.4, 127.2, 121.3, 121.1, 116.3, 116.1, 109.7, 109.6, 49.8, 48.92, 48.86, 48.3, 47.9, 46.0, 45.6, 44.1, 28.2, 26.0; ESI-MS: *m/z* 432.2 $[M+H]^+$; HR-ESI-TOF-MS $[M+H]^+$ calcd. for $C_{25}H_{23}ClN_3O_2$: 432.1473, found: 432.1470.

(4-(5-Chlorobenzo[*d*]oxazol-2-yl)-1,4-diazepan-1-yl)(4-methyl-[1,1'-biphenyl]-2-yl)methanone (**9**)

The synthesis, workup and purification of compound **9** was performed as described for **8**, employing 4-methyl-[1,1'-biphenyl]-2-carboxylic acid (**7**, 50.6 mg, 0.238 mmol), HATU (151.6 mg, 0.399 mmol), DMF (3 mL), DIPEA (170 µL, 0.983 mmol) and 5-chloro-2-(1,4-

diazepan-1-yl)benzo[*d*]oxazole (**5**, 50.3 mg, 0.200 mmol) in DMF (1 mL). Preparative HPLC (t_R = 22.9 min, λ = 220 nm) yielded compound **9** as a white solid (80.8 mg, 91%). Analytical HPLC (220 nm): system 1, purity: >99% (t_R: 24.1 min); ^{1}H-NMR (400 MHz, $CDCl_3$ several rotamers were observed): *δ* (ppm) 7.51-7.43 (m, 2H), 7.40 (d, *J* = 2.0 Hz, 0.5H), 7.38-7.28 (m, 4H), 7.22-7.16 (m, 1.5H), 7.14-7.09 (m, 1H), 7.05 (dd, *J* = 8.5, 2.1 Hz, 0.5H), 7.01 (dd, *J* = 8.5, 2.1 Hz, 0.5H), 6.97-6.94 (m, 0.5H), 6.92-6.87 (m, 0.5H), 4.24-4.13 (m, 0.5H), 3.88-3.74 (m, 1H), 3.74-3.56 (m, 1.5H), 3.56-3.39 (m, 1.5H), 3.39-3.17 (m, 1H), 3.16-2.97 (m, 1.5H), 2.97-2.89 (m, 0.5H), 2.86-2.74 (m, 0.5H), 2.39 (s, 1.5H), 2.30 (s, 1.5H), 2.20-2.08 (m, 0.5H), 1.91-1.78 (m, 0.5H), 1.60-1.46 (m, 0.5H), 1.18-1.05 (m, 0.5H); ^{13}C-NMR (DEPTQ, 151 MHz, $CDCl_3$, several rotamers were observed): *δ* (ppm) 171.9, 171.8, 162.1, 162.0, 147.2, 147.0, 143.6, 143.1, 139.9, 139.6, 138.1, 137.9, 135.48, 135.46, 135.0, 130.6, 130.5, 130.0, 129.9, 129.8, 129.6, 129.0, 128.9, 128.7, 128.5, 127.9, 127.8, 127.7, 127.6, 121.1, 121.0, 116.4, 116.2, 109.6, 109.5, 49.7, 48.9, 48.8, 48.3, 47.9, 45.9, 45.6, 44.1, 28.1, 26.0, 21.1, 21.0; ESI-MS: *m/z* 446.2 $[M+H]^+$; HR-ESI-TOF-MS $[M+H]^+$ calcd. for $C_{26}H_{25}ClN_3O_2$: 446.1630, found: 446.1627.

(4-(5-Chlorobenzo[*d*]oxazol-2-yl)-1,4-diazepan-1-yl)(4'-fluoro-4-methyl-[1,1'-biphenyl]-2-yl)methanone (**10**)

The synthesis, workup, and purification of compound **10** was performed as described for **8**, employing **2.1** (43.9 mg, 0.191 mmol), HATU (123.3 mg, 0.324 mmol), DMF (3 mL), DIPEA (142 µL, 0.810 mmol) and 5-chloro-2-(1,4-diazepan-1-yl)benzo[*d*]oxazole (**5**, 40.8 mg, 0.162 mmol) in DMF (1 mL). Preparative HPLC (t_R = 23.1 min, λ = 220 nm) yielded compound **10** as a white solid (67.1 mg, 89%). Analytical HPLC (220 nm): system 1, purity: >99% (t_R: 24.2 min); ^{1}H-NMR (400 MHz, $CDCl_3$, several rotamers were observed): *δ* (ppm) 7.49-7.40 (m, 2H), 7.31-7.28 (m, 1H), 7.26-7.23 (m, 2H), 7.17-7.07 (m, 1.5H), 7.04-6.94 (m, 3H) 6.89

(brs, 0.5H), 3.94-3.31 (m, 5H), 3.30-2.83 (m, 3H), 2.37 (s, 1.3H), 2.27 (s, 1.7H), 2.22-2.10 (m, 0.5H), 1.88-1.76 (m, 0.5H), 1.63-1.53 (m, 0.5H), 1.36-1.28 (m, 0.5H); ^{13}C-NMR (DEPTQ, 101 MHz, $CDCl_3$, several rotamers were observed): δ (ppm) 171.6, 171.5, 162.6, 162.55 (d, J = 247 Hz), 162.53 (d, J = 247 Hz), 162.3, 147.6, 144.71, 144.68, 138.1, 138.0, 135.9 (d, J = 3 Hz), 135.8 (d, J = 3 Hz), 135.31, 135.27, 134.42, 134.39, 130.6 (d, J = 7 Hz), 130.5 (d, J = 7 Hz), 130.5, 130.4, 129.7, 129.7, 129.6, 129.5, 127.8, 127.7, 120.6, 120.5, 116.5,116.4, 115.51 (d, J = 22 Hz), 115.48 (d, J = 22 Hz), 109.42, 109.39, 49.5, 48.51, 48.47, 48.1, 46.2, 46.1, 44.0, 27.9, 26.5, 21.1, 21.0; ESI-MS: m/z 464.2 $[M+H]^+$; HR-ESI-TOF-MS $[M+H]^+$ calcd. for $C_{26}H_{24}ClFN_3O_2$: 464.1536, found: 464.1537.

(4-(5-Chlorobenzo[*d*]oxazol-2-yl)-1,4-diazepan-1-yl)(3'-fluoro-4-methyl-[1,1'-biphenyl]-2-yl)methanone (**11 (KD10)**)

The synthesis, workup and purification of compound **11** was performed as described for **8**, employing **3.1** (55.3 mg, 0.240 mmol), HATU (152.3 mg, 0.400 mmol), DMF (3 mL), DIPEA (176 µL, 1.00 mmol) and 5-chloro-2-(1,4-diazepan-1-yl)benzo[*d*]oxazole (**5**, 50.4 mg, 0.200 mmol) in DMF (1 mL). Preparative HPLC (t_R = 23.3 min, λ = 220 nm) yielded compound **11** as a white solid (86.7 mg, 93%). Analytical HPLC (220 nm): system 1, purity: >99% (t_R: 24.3 min); ^{1}H-NMR (600 MHz, $CDCl_3$, several rotamers were observed): δ (ppm) 7.49 (d, J = 1.9 Hz, 0.5H), 7.40 (d, J = 1.9 Hz, 0.5H), 7.33-7.10 (m, 7H), 7.08 (dd, J = 8.6, 2.0 Hz, 0.5H), 7.01 (ddd, J = 8.3, 8.3, 2.2 Hz, 0.5H), 6.91 (brs, 0.5H), 6.47 (ddd, J = 8.3, 8.3, 2.2 Hz, 0.5H), 4.28-4.16 (m, 0.5H), 3.96-3.86 (m, 0.5), 3.86-3.75 (m, 1H), 3.73-3.45 (m, 3H), 3.45-3.35 (m, 0.5H), 3.23-3.10 (m, 1H), 3.10-2.90 (m, 1.5H), 2.38 (s, 1.7H), 2.27 (s, 1.3H), 2.23-2.12 (m, 0.5H),1.94-1.83 (m, 0.5H), 1.66-1.53 (m, 0.5H), 1.23-1.08 (m, 0.5H); ^{13}C-NMR (DEPTQ, 151 MHz, $CDCl_3$, several rotamers were observed): δ (ppm) 172.1, 171.9, 162.8 (d, J = 247 Hz), 162.5 (d, J = 247 Hz), 161.0, 160.8, 146.3, 145.9, 141.9 (d, J = 8 Hz), 141.7 (d, J =

8 Hz), 138.8, 138.7, 134.2 (d, *J* = 4 Hz), 134.1 (d, *J* = 4 Hz), 131.02, 131.00, 130.9, 130.6, 130.3 (d, *J* = 8 Hz), 130.2 (d, *J* = 8 Hz), 129.9, 129.6, 127.8, 127.6, 124.7 (d, *J* = 2 Hz), 124.6 (d, *J* = 2 Hz), 122.6, 122.1, 116.0, 115.74 (d, *J* = 22 Hz), 115.70 (d, *J* = 22 Hz), 115.6, 114.8 (d, *J* = 21 Hz), 114.2 (d, *J* = 21 Hz), 110.4, 110.0, 49.8, 49.3, 49.0, 48.3, 47.7, 46.3, 45.0, 44.3, 28.4, 25.8, 21.09, 20.99; ESI-MS: *m/z* 464.3 $[M+H]^+$; HR-ESI-TOF-MS $[M+H]^+$ calcd. for $C_{26}H_{24}ClFN_3O_2$: 464.1536, found: 464.1533.

(4-(5-Chlorobenzo[*d*]oxazol-2-yl)-1,4-diazepan-1-yl)(2'-fluoro-4-methyl-[1,1'-biphenyl]-2-yl)methanone (**12**)

The synthesis, workup and purification of compound **12** was performed as described for **8**, employing **4.1** (54.6 mg, 0.237 mmol), HATU (120.2 mg, 0.316 mmol), DMF (3 mL), DIPEA (139 µL, 0.791 mmol) and 5-chloro-2-(1,4-diazepan-1-yl)benzo[*d*]oxazole (**5**, 39.8 mg, 0.158 mmol) in DMF (1 mL). Preparative HPLC (t_R = 22.9 and 23.3 min, λ = 220 nm) yielded compound **12** as a white solid (66.0 mg, 90%). Analytical HPLC (220 nm): system 1, purity: >99% (t_R: 24.1 min); ^{1}H-NMR (600 MHz, $CDCl_3$, several rotamers were observed): *δ* (ppm) 7.50-7.40 (m, 1H), 7.36-7.23 (m, 3.5H), 7.14(d, *J* = 8.5 Hz, 1H), 7.13-7.09 (m, 1H), 7.07-7.02 (m, 0.5H), 7.02-6.92 (m, 3H), 4.08-3.87 (m, 0.5H), 3.87-3.73 (m, 1H), 3.73-3.51 (m, 2.5H), 3.51-3.40 (m, 1H), 3.40-3.27 (m, 0.5H), 3.24-3.12 (m, 2H), 3.12-3.03 (m, 0.5H), 2.39 (s, 1.5H), 2.31 (s, 1.5H), 2.20-2.08 (m, 0.5H), 1.83-1.76 (m, 0.5H), 1.73-1.62 (m, 0.5H), 1.52-1.34 (m, 0.5H); ^{13}C-NMR (DEPTQ, 151 MHz, $CDCl_3$, several rotamers were observed): *δ* (ppm) 171.0, 162.6, 162.3, 159.60 (d, *J* = 246 Hz), 159.59 (d, *J* = 246 Hz), 147.6, 147.5, 144.6, 138.6, 138.4, 136.1, 136.0, 132.12 (d, *J* = 8 Hz), 132.10 (d, *J* = 8 Hz), 131.2 (d, *J* = 3 Hz), 130.9 (d, *J* = 3 Hz), 129.9, 129.8, 129.7 (d, *J* = 8 Hz), 129.6, 129.5 (d, *J* = 8 Hz), 129.3, 129.2, 127.8, 127.6, 127.2 (d, *J* = 14 Hz), 126.9 (d, *J* = 14 Hz), 124.2 (d, *J* = 3 Hz), 124.1 (d, *J* = 3 Hz), 120.6, 120.5, 116.5, 116.3, 115.80 (d, *J* = 22 Hz), 115.75 (d, *J* = 22 Hz), 109.41,

109.38, 49.8, 48.9, 48.8, 48.3, 47.8, 46.0, 45.9, 44.2, 28.3, 26.2, 21.3, 21.2; ESI-MS: *m/z* 464.2 $[M+H]^+$; HR-ESI-TOF-MS $[M+H]^+$ calcd. for $C_{26}H_{24}ClFN_3O_2$: 464.1536, found: 464.1533.

((*S*)-2-((*S*)-*sec*-Butyl)-4-(5-chlorobenzo[*d*]oxazol-2-yl)-1,4-diazepan-1-yl)(3'-fluoro-4-methyl-[1,1'-biphenyl]-2-yl)methanone (**14 (KD23)**)

To a solution of **3.1** (11.1 mg, 0.048 mmol) and HATU (18.3 mg, 0.048 mmol) in DMF (0.5 mL) was added DIPEA (19 µL, 0.110 mmol). After stirring for 20 min at rt, 2-((*S*)-3-((*S*)-sec-butyl)-1,4-diazepan-1-yl)-5-chlorobenzo[*d*]oxazole (**13**, 13.5 mg, 0.044 mmol) in DMF (0.5 mL) was added and the solution was reacted for 12 h at 50 °C. Purification was done by preparative HPLC using CH_3CN/H_2O, a gradient of 40-83% CH_3CN in 30 min (column 1, t_R = 28.6 and 29.1 min, λ = 220 nm) at a flow rate of 12 mL/min, to obtain compound **14** as a white solid (13.6 mg, 60%). Analytical HPLC (220 nm): system 2, purity: >99% (t_R: 25.0 min and 25.5 min (rotamers)); ^{1}H-NMR (600 MHz, $CDCl_3$, several rotamers were observed): *δ* (ppm) 7.75-6.77 (m, 10H), 4.90-2.58 (m, 6.5H), 2.40 (s, 0.5H), 2.37 (s, 2.5H),1.98-1.76 (m, 1H), 1.71-0.79 (m, 8H), 0.69 (t, *J* = 7 Hz, 0.5H), 0.65-0.37 (m, 2H); ^{13}C-NMR (DEPTQ, 151 MHz, $CDCl_3$, several rotamers were observed): *δ* (ppm) 172.2, 171.9, 171.8, 162.93 (d, *J* = 246 Hz), 162.80 (d, *J* = 246 Hz), 162.77 (d, *J* = 246 Hz), 162.72 (d, *J* = 246 Hz), 147.5, 147.19, 147.15, 142.6 (d, *J* = 7 Hz), 142.1 (d, *J* = 7 Hz), 141.8 (d, *J* = 7 Hz), 138.4, 138.3, 138.2, 138.1, 136.03, 135.96, 135.6, 135.5, 134.1 (d, *J* = 2 Hz), 133.8 (d, *J* = 2 Hz), 133.6 (d, *J* = 2 Hz), 130.22, 130.21, 130.15, 130.13, 130.05 (d, *J* = 8 Hz), 129.96 (d, *J* = 8 Hz), 129.85, 129.79, 129.6, 128.9, 127.8, 127.5, 125.2 (d, *J* = 4 Hz), 124.9 (d, *J* = 4 Hz), 124.8 (d, *J* = 4 Hz), 121.3, 120.8, 120.7, 116.6, 116.35, 116.31, 116.2 (d, *J* = 22 Hz), 116.14 (d, *J* = 22 Hz), 116.11 (d, *J* = 22 Hz), 114.65 (d, *J* = 21 Hz), 114.62 (d, *J* = 21 Hz), 114.57 (d, *J* = 21 Hz), 114.2 (d, *J* = 21 Hz), 109.9, 109.7, 109.5, 109.3, 61.8, 59.9, 56.1, 50.7, 50.3, 49.8, 49.5, 48.9, 43.7, 41.7, 39.6, 37.2, 35.8, 33.8, 28.2, 27.4, 27.0, 26.4, 26.0, 25.9, 25.5, 21.3, 21.21, 21.17, 20.5, 15.5, 15.4, 14.1, 14.0, 11.9, 11.71, 11.68, 11.2; $[\alpha]_D^{24}$: +86.3 (c 0.3, methanol); ESI-MS: *m/z* 520.4 $[M+H]^+$; HR-ESI-TOF-MS $[M+H]^+$ calcd. for $C_{30}H_{32}ClFN_3O_2$: 520.2162, found: 520.2165.

((*S*)-2-((*S*)-*sec*-Butyl)-4-(5-chlorobenzo[*d*]oxazol-2-yl)-1,4-diazepan-1-yl)(2'-fluoro-4-methyl-[1,1'-biphenyl]-2-yl)methanone (**15**)

To a solution of **4.1** (11.1 mg, 0.048 mmol) and HATU (18.3 mg, 0.048 mmol) in DMF (0.5 mL) was added DIPEA (19 µL, 0.110 mmol). After stirring for 20 min at rt, 2-((*S*)-3-((*S*)-sec-butyl)-1,4-diazepan-1-yl)-5-chlorobenzo[*d*]oxazole (**13**, 13.5 mg, 0.044 mmol) in DMF (0.5 mL) was added and the solution was reacted for 12 h at 50 °C. The solvent was removed under reduced pressure. Purification was done by preparative HPLC using CH_3CN/H_2O, a gradient of 40-83% CH_3CN in 30 min (column 1, t_R = 28.0 min, λ = 220 nm) at a flow rate of 12 mL/min, to obtain compound **15** as a white solid (14.9 mg, 65%). Analytical HPLC (220 nm): system 2, purity: >99% (t_R: 25.6 min). ^{1}H-NMR (600 MHz, $CDCl_3$, several rotamers were observed): *δ* (ppm) 7.73-6.36 (m, 10H), 4.87-4.49 (m, 1H), 4.39-3.70 (m, 1.5H), 3.59-3.19 (m, 2.5H), 3.11-2.67 (m, 1.5H), 2.41 (s, 0.5H), 2.38 (s, 2.5H), 2.04-0.42 (m, 11.5H); ^{13}C-NMR (DEPTQ, 151 MHz, $CDCl_3$, several rotamers were observed): *δ* (ppm) 171.8, 171.6, 171.5, 171.48, 162.9, 162.3, 159.7 (d, *J* = 246 Hz), 159.5 (d, *J* = 246 Hz), 147.6, 147.4, 147.3, 138.4, 138.3, 138.1, 138.0, 136.9, 136.8, 136.4, 136.1, 132.8, 132.6, 131.8, 131.5, 131.22, 131.20, 130.8, 129.8 (d, *J* = 8 Hz), 129.6 (d, *J* = 8 Hz), 129.5, 129.4, 129.35, 129.29, 129.2, 128.9, 128.7, 128.4, 127.6, 127.4, 127.1 (d, *J* = 15 Hz), 126.9 (d, *J* = 15 Hz), 124.3 (d, *J* = 4 Hz), 124.0 (d, *J* = 4 Hz), 120.7, 120.53, 120.47, 116.6, 116.34, 116.29, 115.7 (d, *J* = 22 Hz), 115.6 (d, *J* = 22 Hz), 109.6, 109.5, 109.4, 109.3, 61.8, 56.2, 50.7, 50.0, 49.6, 48.7, 43.6, 41.5, 39.5, 37.3, 35.9, 35.7, 33.7, 28.3, 27.3, 26.9, 26.6, 26.1, 25.6, 25.5, 21.33, 21.30, 20.7, 15.5, 15.4, 14.3, 14.0, 11.8, 11.7, 11.5, 11.2; $[\alpha]_D^{24}$: +80.2 (c 1.1, methanol); ESI-MS: *m/z* 520.4 $[M+H]^+$; HR-ESI-TOF-MS $[M+H]^+$ calcd. for $C_{30}H_{32}ClFN_3O_2$: 520.2162, found: 520.2163.

Methyl 3'-bromo-4-methyl-[1,1'-biphenyl]-2-carboxylate (**16**)[37]

To a solution of methyl 2-iodo-5-methylbenzoate (**1**, 150.0 mg, 0.543 mmol) in THF (1.5 mL) was added $PdCl_2(PPh_3)_2$ (11.4 mg, 0.016 mmol) and an aq. solution of Na_2CO_3 (116.3 mg, 1.09 mmol, 3 mL). The mixture was heated to 80 °C. 2-(3-Bromophenyl)-4,4,5,5-tetramethyl-1,3,2-dioxaborolane (184.5 mg, 0.652 mmol) was dissolved in THF (1.5 mL) and added to the reaction mixture over 1 h. After complete addition, the mixture was stirred for 1 h at 80 °C. Extraction was done with ethyl acetate, the organic layer was washed with brine, dried over Na_2SO_4, filtered, and the solvent was removed under reduced pressure. Purification was done by automated flash chromatography (ethyl acetate/isohexane: isocratic elution with 1% ethyl acetate), to obtain compound **16** (114.1 mg, 69%) as a clear oil. ^{1}H-NMR (600 MHz, $CDCl_3$): *δ* (ppm) 7.69-7.65 (m, 1H), 7.49-7.44 (m, 2H), 7.36-7.32 (m, 1H), 7.26-7.22 (m, 2H), 7.22-7.18 (m, 1H), 3.66 (s, 3H), 2.42 (s, 3H); ^{13}C-NMR (DEPTQ, 151 MHz, $CDCl_3$): *δ* (ppm) 168.9, 143.6, 138.3, 137.8, 132.3, 131.5, 130.7, 130.5, 130.2, 129.5, 127.3, 122.1, 52.1, 21.1; ESI-MS: *m/z* 305.2 $[M+H]^+$; HR-ESI-TOF-MS $[M+Na]^+$ calcd. for $C_{15}H_{13}BrNaO_2$: 326.9991, found: 326.9996.

3'-Bromo-4-methyl-[1,1'-biphenyl]-2-carboxylic acid (**17**)[36]

16 (179 mg, 0.588 mmol) was dissolved in a mixture of dioxane (2.4 mL) and methanol (1.6 mL). An aqueous solution of NaOH (588 µL, 2 M) was added. After heating the reaction mixture to 60 °C for 12 h, volatiles were removed under reduced pressure, and pH 3 was adjusted with 0.1 M HCl. Extraction with ethyl acetate was performed and the organic layer was washed with brine, dried over Na_2SO_4, and the solvent was removed under reduced pressure. Purification was done by automated flash chromatography (ethyl acetate/isohexane: isocratic elution with 50% ethyl acetate) to obtain compound **17** (163 mg, 95%) as a white solid. ^{1}H-NMR (600 MHz, $CDCl_3$): *δ* (ppm) 7.80 (dq, *J* = 1.6, 0.5 Hz, 1H), 7.49-7.44 (m, 2H), 7.38 (ddq, *J* = 7.8, 1.6, 0.6 Hz, 1H), 7.27-7.20 (m, 3H), 2.43 (brs, 3H); ^{13}C-NMR (DEPTQ, 151 MHz, $CDCl_3$): *δ* (ppm) 172.4, 143.3, 139.3, 137.9, 133.2, 131.6, 131.5, 131.2, 130.3, 129.6, 128.8, 127.5, 122.1, 21.1; ESI-MS: *m/z* 291.1 $[M+H]^+$; HR-ESI-TOF-MS $[M+H]^+$ calcd.

for $C_{14}H_{12}BrO_2$: 291.0015, found: 291.0016. Analytical data were in accordance with those reported in the literature[36].

(3'-Bromo-4-methyl-[1,1'-biphenyl]-2-yl)(4-(5-chlorobenzo[*d*]oxazol-2-yl)-1,4-diazepan-1-yl)methanone (**18**)

To a solution of **17** (62.3 mg, 0.214 mmol) and HATU (81.4 mg, 0.214 mmol) in DMF (1 mL) was added DIPEA (84 µL, 0.487 mmol). After stirring for 20 min at rt, 5-chloro-2-(1,4-diazepan-1-yl)benzo[*d*]oxazole (**5**, 49.0 mg, 0.195 mmol) in DMF (1 mL) was added and the solution was reacted for 12 h at 50 °C. Purification was done by preparative HPLC using CH_3CN/H_2O, a gradient of 40-65% CH_3CN in 20 min (column 2, t_R = 19.7 min, λ = 220 nm) at a flow rate of 25 mL/min, to obtain compound **18** as a white solid (87.7 mg, 86%). Analytical HPLC (220 nm): system 1, purity: 99% (t_R: 24.0 min); ^{1}H-NMR (400 MHz, $CDCl_3$, several rotamers were observed): *δ* (ppm) 7.63-7.58 (m, 0.5H), 7.57-7.52 (m, 0.5H), 7.40-7.32 (m, 1.5H), 7.28 (d, *J* = 1.8 Hz, 0.5H), 7.25-7.17 (m, 2.5H), 7.17-7.09 (m, 1H), 7.09-6.94 (m, 2.5H), 6.93 (dd, *J* = 8.4, 2.1 Hz, 0.5H), 6.87-6.83 (m, 0.5H), 4.08-3.89 (m, 0.5H), 3.89-3.71 (m, 1H), 3.71-3.39 (m, 3H), 3.39-3.18 (m, 1H), 3.12-3.02 (m, 0.5H), 2.99 (t, *J* = 6.1 Hz, 1H), 2.92-2.76 (m, 1H), 2.31 (s, 1.5H), 2.21 (s, 1.5H), 2.17-2.08 (m, 0.5H), 1.89-1.77 (m, 0.5H), 1.60-1.49 (m, 0.5H), 1.27-1.21 (m, 0.5H); ^{13}C-NMR (DEPTQ, 151 MHz, $CDCl_3$, several rotamers were observed): *δ* (ppm) 171.3, 171.2, 162.3, 162.1, 147.4, 147.2, 142.0, 141.7, 138.7, 138.6, 135.2, 135.17, 139.9, 133.8, 131.7, 131.66, 130.7, 130.6, 130.5, 130.4, 130.2, 130.0, 129.8, 129.77, 129.5, 128.1, 127.7, 127.6, 127.5, 122.7, 122.6, 120.8, 116.4, 116.3, 109.7, 109.5, 49.8, 48.9, 48.5, 47.9, 46.0, 45.7, 44.2, 28.2, 26.1, 21.2, 21.1; ESI-MS: *m/z* 524.4 $[M+H]^+$; HR-ESI-TOF-MS $[M+H]^+$ calcd. for $C_{26}H_{24}BrClN_3O_2$: 524.0735, found: 524.0739.

(3'-Bromo-4-methyl-[1,1'-biphenyl]-2-yl)((*S*)-2-((*S*)-*sec*-butyl)-4-(5-chlorobenzo[*d*]oxazol-2-yl)-1,4-diazepan-1-yl)methanone (**19**)

To a solution of **17** (66.1 mg, 0.227 mmol) and HATU (86.3 mg, 227 mmol) in DMF (1 mL) was added DIPEA (89 µL, 0.516 mmol). After stirring for 20 min at rt, 2-((*S*)-3-((*S*)-sec-butyl)-1,4-diazepan-1-yl)-5-chlorobenzo[*d*]oxazole (**13**, 63.5 mg, 0.206 mmol) in DMF (1 mL) was added and the solution was reacted for 12 h at 50 °C. Purification was done by preparative HPLC using CH_3CN/H_2O, a gradient of 50-95% CH_3CN in 20 min (column 1, t_R = 18.3 min and 18.9 min, λ = 220 nm) at a flow rate of 12 mL/min, to obtain compound **19** as a white solid (78.1 mg, 65%). Analytical HPLC (220 nm): system 2, purity: >99% (t_R: 26.2 min, and 26.8 min, rotamers); ^{1}H-NMR (600 MHz, $CDCl_3$, several rotamers were observed) *δ* (ppm) 7.79-7.58 (m, 1H), 7.58-7.40 (m, 1H), 7.40-7.05 (m, 6H), 7.05-6.81 (m, 2H), 4.96-2.52 (m, 6.5H), 2.40 (s, 0.5H), 2.39 (s, 0.5H), 2.37 (s, 2H), 2.11-1.79 (m, 1H), 1.73-0.80 (m, 8H), 0.69 (t, *J* = 7 Hz, 0.5H), 0.63-0.37 (m, 2H); ^{13}C-NMR (DEPTQ, 151 MHz, $CDCl_3$, several rotamers were observed): *δ* (ppm) 172.1, 171.8, 171.7, 161.8, 147.3, 142.5, 142.0, 141.8, 138.5, 138.2, 138.1, 136.1, 136.0, 135.7, 135.5, 133.8, 133.6, 133.5, 133.2, 132.3, 132.2, 132.00, 131.98, 130.8, 130.7, 130.3, 130.23, 130.20, 130.15, 130.13, 130.10, 130.01, 129.97, 129.8, 129.6, 128.9, 128.11, 128.08, 127.82, 127.77, 127.54, 127.47, 122.7, 122.6, 122.5, 121.1, 120.64, 120.62, 116.6, 116.4, 116.2, 109.8, 109.6, 109.5, 109.3, 62.0, 56.2, 50.7, 50.2, 50.0, 49.8, 49.2, 48.7, 43.8, 41.7, 39.5, 37.3, 35.9, 35.7, 33.7, 28.5, 27.3, 27.0, 26.3, 26.03, 25.99, 25.92, 25.5, 21.3, 21.21, 21.19, 20.6, 15.5, 13.93, 11.87, 11.7, 11.2; $[\alpha]_D^{23}$: +77.9 (c 0.6, methanol); ESI-MS: *m/z* 580.5 $[M+H]^+$; HR-ESI-TOF-MS $[M+H]^+$ calcd. for $C_{30}H_{32}BrClN_3O_2$: 580.1361, found: 580.1365.

(4-(5-Chlorobenzo[*d*]oxazol-2-yl)-1,4-diazepan-1-yl)(4-methyl-3'-(4,4,5,5-tetramethyl-1,3,2-dioxaborolan-2-yl)-[1,1'-biphenyl]-2-yl)methanone (**20**)

To a flask containing 4,4,4',4',5,5,5',5'-octamethyl-2,2'-bi(1,3,2-dioxaborolane) (158.3 mg, 0.623 mmol), Pd(dppf)Cl_2×CH_2Cl_2 (76.4 mg, 0.094 mmol), and KOAc (91.8 mg, 0.935 mmol) a solution of **18** (163.6 mg, 0.312 mmol) in dioxane (1.5 mL) was added. The reaction mixture was stirred for 6 h at 80 °C. Purification was done by automated flash chromatography (CH_3CN/H_2O: isocratic elution with 60% CH_3CN), followed by preparative HPLC using CH_3CN/H_2O, a gradient of 50-70% CH_3CN in 20 min (column 2, t_R = 19.7 min, λ = 220 nm) at a flow rate of 25 mL/min, to obtain compound **20** as a white solid (123.6 mg, 69%). Analytical HPLC (220 nm): system 3, purity: 97% (t_R: 15.6 min); ^{1}H-NMR (600 MHz, CD_3CN, several rotamers were observed): *δ* (ppm) 7.79-7.72 (m, 1H), 7.66-7.62 (m, 0.5H), 7.55-7.51 (m, 0.5H), 7.51-7.47 (m, 0.5H), 7.37-7.32 (m, 2H), 7.32-7.28 (m, 1H), 7.27 (d, *J* = 2.1 Hz, 0.5H), 7.25 (d, *J* = 8.5 Hz, 0.5H), 7.24-7.17 (m, 1.5H), 7.03-6.98 (m, 1.5H), 6.76 (brs, 0.5H), 3.89-3.79 (m, 1H), 3.79-3.69 (m, 1H), 3.69-3.54 (m, 2H), 3.42-3.26 (m, 1.5H), 3.24-3.12 (m, 1H), 3.10-2.95 (m, 1H), 2.91-2.80 (m, 0.5H), 2.33 (s, 1.5H), 2.22 (s, 1.5H), 2.04-1.99 (m, 0.5H), 1.82-1.74 (m, 0.5H), 1.64-1.53 (m, 0.5H), 1.32 (brs, 12H), 1.29-1.22 (m, 0.5H); ^{13}C-NMR (DEPTQ, 151 MHz, CD_3CN, several rotamers were observed): *δ* (ppm) 171.7, 171.6, 164.0, 163.7, 146.3, 146.2, 140.2, 140.1, 138.6, 138.5, 136.8, 136.7, 136.1, 136.0, 135.3, 135.2, 134.4, 134.2, 132.4, 132.3, 130.9, 130.8, 130.5, 130.2, 129.6, 129.5, 129.0, 128.8, 128.7, 128.3, 120.8, 120.6, 116.5, 116.4, 110.5, 110.4, 84.9, 84.85, 49.6, 49.4, 49.2, 48.6, 47.9, 46.5, 45.5, 44.4, 28.8, 26.8, 25.2, 25.1, 20.9, 20.87; ESI-MS: *m/z* 572.4 $[M+H]^+$; HR-ESI-TOF-MS $[M+H]^+$ calcd. for $C_{32}H_{36}BClN_3O_4$: 572.2482, found: 572.2488.

((*S*)-2-((*S*)-*sec*-Butyl)-4-(5-chlorobenzo[*d*]oxazol-2-yl)-1,4-diazepan-1-yl)(4-methyl-3'-(4,4,5,5-tetramethyl-1,3,2-dioxaborolan-2-yl)-[1,1'-biphenyl]-2-yl)methanone (**21**)

To a flask containing 4,4,4',4',5,5,5',5'-octamethyl-2,2'-bi(1,3,2-dioxaborolane) (68.3 mg, 0.269 mmol), Pd(dppf)Cl_2×CH_2Cl_2 (32.9 mg, 0.040 mmol), and KOAc (39.6 mg, 0.403 mmol)

a solution of **19** (78.1 mg, 0.134 mmol) in dioxane (1.5 mL) was added. The reaction mixture was stirred for 6 h at 80 °C. Purification was done by automated flash chromatography (CH_3CN/H_2O: gradient 65-79% CH_3CN), followed by preparative HPLC using CH_3CN/H_2O, a gradient of 60-90% CH_3CN in 20 min (column 2, t_R = 17.1 min and 17.6 min, λ = 220 nm) at a flow rate of 25 mL/min, to obtain compound **21** as a white solid (52.9 mg, 63%). Analytical HPLC (220 nm): system 3, purity: 96% (t_R: 17.7 and 18.3 min, rotamers); ^{1}H-NMR (600 MHz, CD_3CN, several rotamers were observed): *δ* (ppm) 7.89-7.60 (m, 2H), 7.56-7.09 (m, 6H), 7.07-6.69 (m, 1H), 6.93-6.79 (m, 1H), 4.89-2.77 (m, 6.5H), 2.38 (s, 0.5H), 2.33 (s, 2H), 2.14-2.03 (m, 0.5H), 1.83-0.37 (m, 23.5H); ^{13}C-NMR (DEPTQ, 151 MHz, CD_3CN, several rotamers were observed): *δ* (ppm) 172.5, 172.47, 172.24, 172.2, 164.1, 163.6, 163.4, 148.8, 148.6, 148.6, 146.3,4, 146.28, 140.5, 140.33, 139.6, 138.4, 138.29, 138.26, 138.1, 137.45, 137.39, 137.0, 136.8, 136.1, 136.0, 135.91, 135.87, 135.7, 135.5, 135.1, 135.0, 134.7, 134.6, 134.4, 134.2, 132.9, 132.81, 132.76, 132.4, 131.0, 130.9, 130.6, 130.5, 130.4, 129.9, 129.8, 129.7, 129.6, 129.5, 129.0, 128.8, 128.6, 128.5, 128.2, 128.0, 120.9, 120.8, 120.52, 120.49, 116.7, 116.43, 116.35, 116.3, 110.6, 110.5, 110.4, 84.8, 61.4, 55.4, 50.8, 50.2, 49.6, 49.5, 49.2, 49.0, 44.4, 42.5, 40.6, 38.1, 37.0, 36.7, 35.1, 28.9, 27.5, 26.91, 26.88, 26.4, 25.23, 25.2, 25.15, 25.10, 25.0, 21.0, 20.9, 20.4, 15.2, 14.7, 13.6, 11.9, 11.8, 11.4 ; ESI-MS: *m/z* 629.0 $[M+H]^+$; HR-ESI-TOF-MS $[M+H]^+$ calcd. for $C_{36}H_{44}BClN_3O_4$: 628.3108, found: 628.3110.

4.3 Radioligand binding

Binding affinities towards the human orexin receptor subtypes OX1R and OX2R were determined as described previously.[20, 29] In brief, membranes were prepared from HEK293T cells transiently transfected with the cDNA for the GPCR (OX1R: human HCRTR1 from cDNA Resource Center, Bloomsburg University, Bloomsberg, PA; OX2R: human HCRTR2 from Genscript, Piscataway, NJ). Homogenates were used with receptor densities (B_{max} value) of 4,100±1,800 fmol/mg protein for OX1R and 1,500±420 fmol/mg protein for OX2R and binding affinities (K_D value) of 0.56±0.04 nM for OX1R and 0.68±0.02 nM for OX2R. Competition

binding experiments were conducted by incubating membranes in binding buffer (50 mM Tris, 5 mM $MgCl_2$, 0.1 mM EDTA, 5 µg/mL bacitracin and 5 µg/mL soybean trypsin inhibitor at pH 7.4) at final protein concentrations of 6 µg/well (OX1R) and 12 µg/well (OX2R) together with the OX1R specific radioligand [^{3}H]SB674042 (specific binding 43 Ci/mmol; final concentration 0.6 nM) and the OX2R radioligand [^{3}H]EMPA (specific binding 84 Ci/mmol; final concentration 0.7 nM) (both purchased from Novandi, Södertälje, Sweden) and varying concentrations of the competing test compounds. After an incubation for 60 min at 37° C bound radioactivity was separated by filtration on GF/B glass fiber mats and counted with a scintillation counter (Microbeta from PerkinElmer, Rodgau, Germany). Non-specific binding was determined in the presence of non-labeled SB674042 and EMPA at a final concentration of 10 µM. The protein concentration was determined applying the method of Lowry.[38] The resulting competition curves were analyzed by nonlinear regression using the algorithms implemented in PRISM 10.2 (GraphPad Software, San Diego, CA) to get IC_{50} values, which were subsequently transformed into the K_i values employing the equation of Cheng and Prusoff.[39]

4.4 Computational chemistry

4.4.1 Molecular docking

Molecular docking was conducted using Glide[40] (Schördinger Suite 2024.1) The LigPrep model was employed to generate corresponding low-energy structures of the ligands **JH112**, **KD23**, and **19** while retaining the chiral centers. For the **JH112**-bound OX1R structure (PDB: 6V9S)[20], the Protein Preparation Wizard module was utilized to optimize the hydrogen bonds of amino acids and model them in their predominant protonation state at pH 7.4. Specifically, H216$^{5.39}$ and H344$^{7.39}$ were protonated due to their proximity to D107$^{2.65}$ and E204$^{45.52}$, respectively. The receptor grid for docking was generated at the centroid of **JH112** with dimensions of 25 × 25 × 25 Å^3. Standard precision was employed for docking, and core constraints on the maximum common substructure (MCS) of **JH112** were applied with a tolerance of 2 Å.

4.4.2 Molecular dynamics simulations

The simulations were conducted based on the high-resolution crystal structure of OX1R in complex with **JH112** (PDB: 6V9S)[20].To prepare the coordinates, all atoms except those of the receptor were removed. Sodium ions were incorporated into the allosteric binding site[41] by superimposing another OX1R structure (PDB: 6TO7)[35] onto our model and extracting the sodium coordinates. To address introduced mutations (A133K and V319I), they were reverted back to their original states. Additionally, the missing portion of the long and flexible intracellular loop 3 (ICL3) was modeled using the sequence GSGSGS, implemented with MODELLER[42].

The Membrane Builder of CHARMM-GUI[43] was used to (a) cap the N and C terminus with acetyl and methylamid groups respectively; (b) protonate H216$^{5.39}$ and H344$^{7.39}$ while keeping all other titratable residues in their predominant protonation state at pH 7.0; (c) bridge C119$^{3.25}$ and C202$^{45.50}$ by disulfide bonds; (d) embed the OX1R receptor model into a palmitoyl-2-oleoyl-*sn*-glycero-3-phosphocholine (POPC) bilayer of approximately 80 Å in the X and Y dimension; (e) solvate the system in a rectangular water box made of explicit water molecules with a water thickness of 22.5 Å surrounding the protein in the Z dimension (f) neutralize the global electrostatic charge and establish a 0.15 M NaCl concentration; (g) parameterized the system using the AMBER force field (ff19SB[44] for proteins, Lipid21[45] for lipids and the OPC water model[46]).

Ligand coordinates were extracted from the previous docking experiments after the OX1R-ligand complexes were superimposed on the system prepared with CHARMM-GUI. The ligands were parameterized using Sage (OpenFF 2.1.0[47]). The topology and coordinates of the system and the ligands were manually combined for each ligand to generate the final system. The final dimensions of the simulation system were about 80 × 80 × 125 Å^3 containing about 91.000 atoms, including 155 POPC molecules, about 16.000 water molecules, 44 sodium ions, and 58 chlorine ions.

Simulations were performed using GROMACS 2024.1[48]. Each system was energy minimized and equilibrated in the NVT ensemble for 1 ns followed by the NPT ensemble for 1 ns with harmonic restraints of 10.0 kcal·mol^{-1}·Å^{-2} on the protein and ligand heavy atoms. Subsequently, the system was further equilibrated in the NPT ensemble for 25 ns with restraints on protein backbone and ligand heavy atoms in which the restraints were reduced every 5 ns in a stepwise fashion to be 10.0, 5.0, 1.0, 0.5, and 0.1 kcal·mol^{-1}·Å^{-2}, respectively. Restraints on the membrane were gradually released following the CHARMM-GUI Membrane Builder protocol. Temperature was coupled the following – (a) thermostat: velocity-rescale[49]; (b) time constant: 1.0 ps; (c) reference temperature: 310 K and pressure was coupled the following – (a) barostat: stochastic cell rescaling[50]; (b) type: semi-isotropic; (c) time constant: 5.0 ps; (d) reference pressure: 1 bar; (e) compressibility: 4.5 × 10^{-5} bar^{-1}. Bond lengths to hydrogen atoms were constrained using LINCES[51] algorithm. Periodic boundary conditions were applied. A cutoff of 10.0 Å was used for Lennard-Jones interactions and the short-range electrostatic interactions. Long-range electrostatics were computed using the particle mesh Ewald (PME)[52] method with a fourth-order interpolation scheme and fast Fourier transform (FFT) grid spacing of 1.25 Å. A continuum model correction for energy and pressure was applied to long-range van der Waals interactions. The equations of motion were integrated with a time step of 2 fs.

Production simulations were performed in the NPT ensemble for a duration of 3 µs. Four replicas were initiated for each conformation, binding mode, and ligand, resulting in a total of 36 simulations.

Figures of the structure and model were prepared with PyMOL 2.4.1[26] and UCSF ChimeraX 1.7.1[53]. Analysis of the trajectories was performed using Visual Molecular Dynamics (VMD)[54] and CPPTRAJ[55]. Plots were created using Matplotlib 3.8.3[56] and Seaborn 0.13.2[57].

Declaration of competing interest

The authors declare that they have no known competing financial interests or personal relationships that could have appeared to influence the work reported in this paper.

Funding

This work was supported by Deutsche Forschungsgemeinschaft (Gm 13/13-1 and PR 677/8-1), the Elitenetzwerk Bayern (Marianne-Plehn-Programm, E.N.), the Verband der Chemischen Industrie (Kekulé fellowship, E.N.) and the Studienstiftung des Deutschen Volkes (E.N.). MD calculations were performed at the NHR cluster at FAU (grant: b132dc).

Acknowledgments

Figures in the graphical abstract were created with BioRender.com and UCSF ChimeraX, developed by the Resource for Biocomputing, Visualization, and Informatics at the University of California, San Francisco, with support from the National Institutes of Health R01-GM129325 and the Office of Cyber Infrastructure and Computational Biology, National Institute of Allergy and Infectious Diseases.

References

[1] Li J, Hu Z, De Lecea L. The hypocretins/orexins: integrators of multiple physiological functions. *Br J Pharmacol*. **2014**;171:332-350. https://doi.org/10.1111/bph.12415.

[2] Wang C, Wang Q, Ji B, Pan Y, Xu C, Cheng B, Bai B, Chen J. The Orexin/Receptor System: Molecular Mechanism and Therapeutic Potential for Neurological Diseases. *Front Mol Neurosci*. **2018**;11:220. https://doi.org/10.3389/fnmol.2018.00220.

[3] Lin L, Faraco J, Li R, Kadotani H, Rogers W, Lin X, Qiu X, De Jong PJ, Nishino S, Mignot E. The Sleep Disorder Canine Narcolepsy Is Caused by a Mutation in the Hypocretin (Orexin) Receptor 2 Gene. *Cell*. **1999**;98:365-376. https://doi.org/10.1016/s0092-8674(00)81965-0.

[4] Chemelli RM, Willie JT, Sinton CM, Elmquist JK, Scammell T, Lee C, Richardson JA, Williams SC, Xiong Y, Kisanuki Y, Fitch TE, Nakazato M, Hammer RE, Saper CB, Yanagisawa M. Narcolepsy in orexin Knockout Mice. *Cell*. **1999**;98:437-451. https://doi.org/10.1016/s0092-8674(00)81973-x.

[5] Nishino S, Ripley B, Overeem S, Lammers GJ, Mignot E. Hypocretin (orexin) deficiency in human narcolepsy. *Lancet*. **2000**;355:39-40. https://doi.org/10.1016/S0140-6736(99)05582-8.

[6] Tsujino N, Sakurai T. Orexin/Hypocretin: A Neuropeptide at the Interface of Sleep, Energy Homeostasis, and Reward System. *Pharmacol Rev*. **2009**;61:162-176. https://doi.org/10.1124/pr.109.001321.

[7] Chiou L-C, Lee H-J, Ho Y-C, Chen S-P, Liao Y-Y, Ma C-H, Fan P-C, Fuh J-L, Wang S-J. Orexins/Hypocretins: Pain Regulation and Cellular Actions. *Curr Pharm Des*. **2010**;16:3089-3100. https://doi.org/10.2174/138161210793292483.

[8] Bingham S, Davey PT, Babbs AJ, Irving EA, Sammons MJ, Wyles M, Jeffrey P, Cutler L, Riba I, Johns A, Porter RA, Upton N, Hunter AJ, Parsons AA. Orexin-A, an hypothalamic peptide with analgesic properties. *Pain*. **2001**;92:81-90. https://doi.org/10.1016/s0304-3959(00)00470-x.

[9] Zischler J, Kolks N, Modemann D, Neumaier B, Zlatopolskiy BD. Alcohol-Enhanced Cu-Mediated Radiofluorination. *Chem - Eur J*. **2017**;23:3251-3256. https://doi.org/10.1002/chem.201604633.

[10] Nerella SG, Singh P, Sanam T, Digwal CS. PET Molecular Imaging in Drug Development: The Imaging and Chemistry Perspective. *Frontiers in Medicine*. **2022**;9:https://doi.org/10.3389/fmed.2022.812270.

[11] Son H, Jang K, Lee H, Kim SE, Kang KW, Lee H. Use of Molecular Imaging in Clinical Drug Development: a Systematic Review. *Nucl Med Mol Imaging (2010)*. **2019**;53:208-215. https://doi.org/10.1007/s13139-019-00593-y.

[12] Wang C, Moseley CK, Carlin SM, Wilson CM, Neelamegam R, Hooker JM. Radiosynthesis and evaluation of [^{11}C]EMPA as a potential PET tracer for orexin 2 receptors. *Bioorg Med Chem Lett*. **2013**;23:3389-3392. https://doi.org/10.1016/j.bmcl.2013.03.079.

[13] Liu F, Majo VJ, Prabhakaran J, Castrillion J, Mann JJ, Martinez D, Kumar JSD. Radiosynthesis of [^{11}C]BBAC and [^{11}C]BBPC as potential PET tracers for orexin2 receptors. *Bioorg Med Chem Lett*. **2012**;22:2172-2174. https://doi.org/10.1016/j.bmcl.2012.01.114.

[14] Rong J, Yamasaki T, Li Y, Kumata K, Zhao C, Haider A, Chen J, Xiao Z, Fujinaga M, Hu K, Mori W, Zhang Y, Xie L, Zhou X, Collier TL, Zhang M-R, Liang S. Development of Novel ^{11}C-Labeled Selective Orexin-2 Receptor Radioligands for Positron Emission Tomography

Imaging. *ACS Med Chem Lett*. **2023**;14:1419-1426. https://doi.org/10.1021/acsmedchemlett.3c00320.
[15] Wang C, Wilson CM, Moseley CK, Carlin SM, Hsu S, Arabasz G, Schroeder FA, Sander CY, Hooker JM. Evaluation of potential PET imaging probes for the orexin 2 receptors. *Nucl Med Biol*. **2013**;40:1000-1005. https://doi.org/10.1016/j.nucmedbio.2013.07.001.
[16] Bai P, Liu Y, Xu Y, Striar R, Yuan G, Afshar S, Langan AG, Rattray AK, Wang C. Synthesis and characterization of a new Positron emission tomography probe for orexin 2 receptors neuroimaging. *Bioorg Chem*. **2022**;123:105779. https://doi.org/10.1016/j.bioorg.2022.105779.
[17] Watanabe H, Fukui K, Shimizu Y, Idoko Y, Nakamoto Y, Togashi K, Saji H, Ono M. Synthesis and biological evaluation of F-18 labeled tetrahydroisoquinoline derivatives targeting orexin 1 receptor. *Bioorg Med Chem Lett*. **2019**;29:1620-1623. https://doi.org/10.1016/j.bmcl.2019.04.044.
[18] Watanabe H, Idoko Y, Iikuni S, Ide T, Shimizu Y, Nakamoto Y, Ono M. Synthesis and biological evaluation of novel ^{18}F-labeled phenylbenzofuran-2-carboxamide derivative for detection of orexin 1 receptor in the brain. *Bioorg Med Chem Lett*. **2021**;43:128098. https://doi.org/10.1016/j.bmcl.2021.128098.
[19] Bai P, Bai S, Placzek MS, Lu X, Fiedler SA, Ntaganda B, Wey H-Y, Wang C. A New Positron Emission Tomography Probe for Orexin Receptors Neuroimaging. *Molecules*. **2020**;25:1018. https://doi.org/10.3390/molecules25051018.
[20] Hellmann J, Drabek M, Yin J, Gunera J, Pröll T, Kraus F, Langmead CJ, Hübner H, Weikert D, Kolb P, Rosenbaum DM, Gmeiner P. Structure-based development of a subtype-selective orexin 1 receptor antagonist. *Proc Natl Acad Sci U S A*. **2020**;117:18059-18067. https://doi.org/10.1073/pnas.2002704117.
[21] Michelson D, Snyder E, Paradis E, Chengan-Liu M, Snavely DB, Hutzelmann J, Walsh JK, Krystal AD, Benca RM, Cohn M, Lines C, Roth T, Herring WJ. Safety and efficacy of suvorexant during 1-year treatment of insomnia with subsequent abrupt treatment discontinuation: a phase 3 randomised, double-blind, placebo-controlled trial. *Lancet Neurol*. **2014**;13:461-471. https://doi.org/10.1016/S1474-4422(14)70053-5.
[22] Yin J, Babaoglu K, Brautigam CA, Clark L, Shao Z, Scheuermann TH, Harrell CM, Gotter AL, Roecker AJ, Winrow CJ, Renger JJ, Coleman PJ, Rosenbaum DM. Structure and ligand-binding mechanism of the human OX1 and OX2 orexin receptors. *Nat Struct Mol Biol*. **2016**;23:293-299. https://doi.org/10.1038/nsmb.3183.
[23] Yin J, Mobarec JC, Kolb P, Rosenbaum DM. Crystal structure of the human OX2 orexin receptor bound to the insomnia drug suvorexant. *Nature*. **2015**;519:247-250. https://doi.org/10.1038/nature14035.
[24] Isberg V, De Graaf C, Bortolato A, Cherezov V, Katritch V, Marshall FH, Mordalski S, Pin J-P, Stevens RC, Vriend G, Gloriam DE. Generic GPCR residue numbers – aligning topology maps while minding the gaps. *Trends Pharmacol Sci*. **2015**;36:22-31. https://doi.org/10.1016/j.tips.2014.11.001.
[25] Ballesteros JA, Weinstein H. Integrated methods for the construction of three-dimensional models and computational probing of structure-function relations in G protein-coupled receptors. In: Sealfon SC, ed. *Methods in Neurosciences*. New York, NY: Academic Press; **1995**:366-428. https://doi.org/10.1016/S1043-9471(05)80049-7.
[26] Schrödinger, LLC, The PyMOL Molecular Graphics System, Version 1.8, **2015**.

[27] Ramirez NP, Bosque I, Gonzalez-Gomez JC. Photocatalytic Dehydrogenative Lactonization of 2-Arylbenzoic Acids. *Org Lett*. **2015**;17:4550-4553. https://doi.org/10.1021/acs.orglett.5b02269.
[28] Shinde SS, Bolik K-V, Maschauer S, Prante O. ^{18}F-Fluorination Using Tri-*Tert*-Butanol Ammonium Iodide as Phase-Transfer Catalyst: An Alternative Minimalist Approach. *Pharmaceuticals*. **2021**;14:833. https://doi.org/10.3390/ph14090833.
[29] Hübner H, Haubmann C, Utz W, Gmeiner P. Conjugated enynes as nonaromatic catechol bioisosteres: synthesis, binding experiments, and computational studies of novel dopamine receptor agonists recognizing preferentially the D_3 subtype. *J Med Chem*. **2000**;43:756-762. https://doi.org/10.1021/jm991098z.
[30] Bolin JT, Filman DJ, Matthews DA, Hamlin RC, Kraut J. Crystal structures of Escherichia coli and Lactobacillus casei dihydrofolate reductase refined at 1.7 A resolution. I. General features and binding of methotrexate. *J Biol Chem*. **1982**;257:13650-13662. https://doi.org/10.1016/S0021-9258(18)33497-5.
[31] Stoll V, Stewart KD, Maring CJ, Muchmore S, Giranda V, Gu Y-GY, Wang G, Chen Y, Sun M, Zhao C, Kennedy AL, Madigan DL, Xu Y, Saldivar A, Kati W, Laver G, Sowin T, Sham HL, Greer J, Kempf D. Influenza Neuraminidase Inhibitors: Structure-Based Design of a Novel Inhibitor Series. *Biochemistry*. **2003**;42:718-727. https://doi.org/10.1021/bi0205449.
[32] Klebe G, Wirkstoffdesign: Entwurf und Wirkung von Arzneistoffen, Springer Spektrum, Berlin, Heidelberg, Germany, **2023**.
[33] Xu P, Huang S, Zhang H, Mao C, Zhou XE, Cheng X, Simon IA, Shen D-D, Yen H-Y, Robinson CV, Harpsøe K, Svensson B, Guo J, Jiang H, Gloriam DE, Melcher K, Jiang Y, Zhang Y, Xu HE. Structural insights into the lipid and ligand regulation of serotonin receptors. *Nature*. **2021**;592:469-473. https://doi.org/10.1038/s41586-021-03376-8.
[34] Chen Z, Fan L, Wang H, Yu J, Lu D, Qi J, Nie F, Luo Z, Liu Z, Cheng J, Wang S. Structure-based design of a novel third-generation antipsychotic drug lead with potential antidepressant properties. *Nat Neurosci*. **2022**;25:39-49. https://doi.org/10.1038/s41593-021-00971-w.
[35] Rappas M, Ali AAE, Bennett KA, Brown JD, Bucknell SJ, Congreve M, Cooke RM, Cseke G, De Graaf C, Doré AS, Errey JC, Jazayeri A, Marshall FH, Mason JS, Mould R, Patel JC, Tehan BG, Weir M, Christopher JA. Comparison of Orexin 1 and Orexin 2 Ligand Binding Modes Using X-ray Crystallography and Computational Analysis. *J Med Chem*. **2020**;63:1528-1543. https://doi.org/10.1021/acs.jmedchem.9b01787.
[36] Wu Z, Chen S, Hu C, Li Z, Xiang H, Zhou X. Palladium-Catalyzed C-H *ortho* Arylation of Benzoic Acids with Diaryliodonium Salts in Water. *ChemCatChem*. **2013**;5:2839-2842. https://doi.org/10.1002/cctc.201300470.
[37] Wei Y, Duan A, Tang P-T, Li J-W, Peng R-M, Zhou Z-X, Luo X-P, Kurmoo M, Liu Y-J, Zeng M-H. Remote and Selective C(sp^2)–H Olefination for Sequential Regioselective Linkage of Phenanthrenes. *Org Lett*. **2020**;22:4129-4134. https://doi.org/10.1021/acs.orglett.0c01208.
[38] Lowry O, Rosebrough N, Farr AL, Randall R. PROTEIN MEASUREMENT WITH THE FOLIN PHENOL REAGENT. *J Biol Chem*. **1951**;193:265-275. https://doi.org/10.1016/S0021-9258(19)52451-6.
[39] Yung-Chi C, Prusoff WH. Relationship between the inhibition constant (K_I) and the concentration of inhibitor which causes 50 per cent inhibition (I_{50}) of an enzymatic reaction. *Biochem Pharmacol*. **1973**;22:3099-3108. https://doi.org/10.1016/0006-2952(73)90196-2.

[40] Friesner RA, Banks JL, Murphy RB, Halgren TA, Klicic JJ, Mainz DT, Repasky MP, Knoll EH, Shelley M, Perry JK, Shaw DE, Francis P, Shenkin PS. Glide: A New Approach for Rapid, Accurate Docking and Scoring. 1. Method and Assessment of Docking Accuracy. *J Med Chem*. **2004**;47:1739-1749. https://doi.org/10.1021/jm0306430.
[41] Katritch V, Fenalti G, Abola EE, Roth BL, Cherezov V, Stevens RC. Allosteric sodium in class A GPCR signaling. *Trends Biochem Sci*. **2014**;39:233-244. https://doi.org/10.1016/j.tibs.2014.03.002.
[42] Šali A, Blundell TL. Comparative Protein Modelling by Satisfaction of Spatial Restraints. *J Mol Biol*. **1993**;234:779-815. https://doi.org/10.1006/jmbi.1993.1626.
[43] Lee J, Cheng X, Swails JM, Yeom MS, Eastman PK, Lemkul JA, Wei S, Buckner J, Jeong JC, Qi Y, Jo S, Pande VS, Case DA, Brooks CL, Mackerell AD, Klauda JB, Im W. CHARMM-GUI Input Generator for NAMD, GROMACS, AMBER, OpenMM, and CHARMM/OpenMM Simulations Using the CHARMM36 Additive Force Field. *J Chem Theory Comput*. **2016**;12:405-413. https://doi.org/10.1021/acs.jctc.5b00935.
[44] Tian C, Kasavajhala K, Belfon KAA, Raguette L, Huang H, Migues AN, Bickel J, Wang Y, Pincay J, Wu Q, Simmerling C. ff19SB: Amino-Acid-Specific Protein Backbone Parameters Trained against Quantum Mechanics Energy Surfaces in Solution. *J Chem Theory Comput*. **2020**;16:528-552. https://doi.org/10.1021/acs.jctc.9b00591.
[45] Dickson CJ, Walker RC, Gould IR. Lipid21: Complex Lipid Membrane Simulations with AMBER. *J Chem Theory Comput*. **2022**;18:1726-1736. https://doi.org/10.1021/acs.jctc.1c01217.
[46] Izadi S, Anandakrishnan R, Onufriev AV. Building Water Models: A Different Approach. *J Phys Chem Lett*. **2014**;5:3863-3871. https://doi.org/10.1021/jz501780a.
[47] Boothroyd S, Behara PK, Madin OC, Hahn DF, Jang H, Gapsys V, Wagner JR, Horton JT, Dotson DL, Thompson MW, Maat J, Gokey T, Wang L-P, Cole DJ, Gilson MK, Chodera JD, Bayly CI, Shirts MR, Mobley DL. Development and Benchmarking of Open Force Field 2.0.0: The Sage Small Molecule Force Field. *J Chem Theory Comput*. **2023**;19:3251-3275. https://doi.org/10.1021/acs.jctc.3c00039.
[48] Abraham MJ, Murtola T, Schulz R, Páll S, Smith JC, Hess B, Lindahl E. GROMACS: High performance molecular simulations through multi-level parallelism from laptops to supercomputers. *SoftwareX*. **2015**;1-2:19-25. https://doi.org/10.1016/j.softx.2015.06.001.
[49] Bussi G, Donadio D, Parrinello M. Canonical sampling through velocity rescaling. *J Chem Phys*. **2007**;126:014101. https://doi.org/10.1063/1.2408420.
[50] Bernetti M, Bussi G. Pressure control using stochastic cell rescaling. *J Chem Phys*. **2020**;153:114107. https://doi.org/10.1063/5.0020514.
[51] Hess B, Bekker H, Berendsen HJC, Fraaije JGEM. LINCS: A linear constraint solver for molecular simulations. *J Comput Chem*. **1997**;18:1463-1472. https://doi.org/10.1002/(SICI)1096-987X(199709)18:12<1463::AID-JCC4>3.0.CO;2-H.
[52] Darden T, York D, Pedersen L. Particle mesh Ewald: An *N*·log(*N*) method for Ewald sums in large systems. *J Chem Phys*. **1993**;98:10089-10092. https://doi.org/10.1063/1.464397.
[53] Meng EC, Goddard TD, Pettersen EF, Couch GS, Pearson ZJ, Morris JH, Ferrin TE. UCSF ChimeraX: Tools for structure building and analysis. *Protein Sci*. **2023**;32:https://doi.org/10.1002/pro.4792.
[54] Humphrey W, Dalke A, Schulten K. VMD: Visual molecular dynamics. *J Mol Graphics*. **1996**;14:33-38. https://doi.org/10.1016/0263-7855(96)00018-5.

[55] Case DA, Aktulga HM, Belfon K, Cerutti DS, Cisneros GA, Cruzeiro VWD, Forouzesh N, Giese TJ, Götz AW, Gohlke H, Izadi S, Kasavajhala K, Kaymak MC, King E, Kurtzman T, Lee T-S, Li P, Liu J, Luchko T, Luo R, Manathunga M, Machado MR, Nguyen HM, O'Hearn KA, Onufriev AV, Pan F, Pantano S, Qi R, Rahnamoun A, Risheh A, Schott-Verdugo S, Shajan A, Swails J, Wang J, Wei H, Wu X, Wu Y, Zhang S, Zhao S, Zhu Q, Cheatham TE, Roe DR, Roitberg A, Simmerling C, York DM, Nagan MC, Merz KM. AmberTools. *J Chem Inf Model*. **2023**;63:6183-6191. https://doi.org/10.1021/acs.jcim.3c01153.

[56] Hunter JD. Matplotlib: A 2D graphics environment. *Comput Sci Eng*. **2007**;9:90-95. https://doi.org/10.1109/Mcse.2007.55.

[57] Waskom M. seaborn: statistical data visualization. *J Open Source Softw*. **2021**;6:3021. https://doi.org/10.21105/joss.03021.